A disynaptic circuit in the globus pallidus controls locomotion inhibition

Asier Aristieta, Massimo Barresi, Shiva Azizpour Lindi, Grégory Barrière, Gilles Courtand, Brice de La Crompe, Lise Guilhemsang, Sophie Gauthier, Stéphanie Fioramonti, Jérôme Baufreton, et al.

Article

Current Biology

A Disynaptic Circuit in the Globus Pallidus Controls Locomotion Inhibition

Graphical Abstract

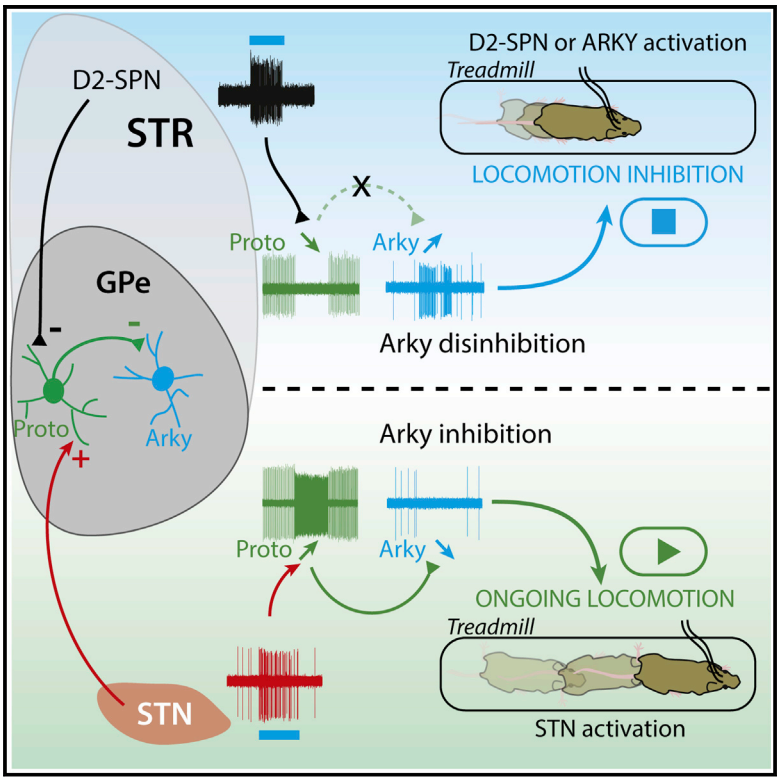

Highlights

- STR and STN inputs are differentially integrated by Proto and Arky GPe neurons
- Axon collaterals of Proto GPe neurons form a disynaptic circuit motif within the GPe
- STR inputs can gate the synaptic integration of STN inputs by Arky GPe neurons
- Disynaptic disinhibition of Arky GPe neurons supports global motor suppression

Authors

Asier Aristieta, Massimo Barresi, Shiva Azizpour Lindi, ..., Stéphanie Fioramonti, Jérôme Baufreton, Nicolas P. Mallet

Correspondence

jerome.baufreton@u-bordeaux.fr (J.B.), nicolas.mallet@u-bordeaux.fr (N.P.M.)

In Brief

Aristieta et al. show that striatal indirect and subthalamic nucleus input organizations present cell-type-specific integration in the external globus pallidus leading to opposite activity patterns between prototypic and arkypallidal neurons and opposite behavioral outcomes on movement inhibition during locomotor activity.

Aristieta et al., 2021, Current Biology *31*, 1–15
February 22, 2021
https://doi.org/10.1016/j.cub.2020.11.019

CellPress

Please cite this article in press as: Aristieta et al., A Disynaptic Circuit in the Globus Pallidus Controls Locomotion Inhibition, Current Biology (2020), https://doi.org/10.1016/j.cub.2020.11.019

Current Biology

CellPress
OPEN ACCESS

Article

A Disynaptic Circuit in the Globus Pallidus Controls Locomotion Inhibition

Asier Aristieta,[1,2] Massimo Barresi,[1,2] Shiva Azizpour Lindi,[1,2] Grégory Barrière,[3] Gilles Courtand,[3] Brice de la Crompe,[1,2] Lise Guilhemsang,[1,2] Sophie Gauthier,[1,2] Stéphanie Fioramonti,[1,2] Jérôme Baufreton,[1,2,4,*] and Nicolas P. Mallet[1,2,4,5,*]
[1]Université de Bordeaux, Institut des Maladies Neurodégénératives, 33076 Bordeaux, France
[2]CNRS UMR 5293, Institut des Maladies Neurodégénératives, 33076 Bordeaux, France
[3]Université de Bordeaux, CNRS UMR 5287, INCIA, 33076 Bordeaux, France
[4]These authors contributed equally
[5]Lead Contact
*Correspondence: jerome.baufreton@u-bordeaux.fr (J.B.), nicolas.mallet@u-bordeaux.fr (N.P.M.)
https://doi.org/10.1016/j.cub.2020.11.019

SUMMARY

The basal ganglia (BG) inhibit movements through two independent circuits: the striatal neuron-indirect and the subthalamic nucleus-hyperdirect pathways. These pathways exert opposite effects onto external globus pallidus (GPe) neurons, whose functional importance as a relay has changed drastically with the discovery of two distinct cell types, namely the prototypic and the arkypallidal neurons. However, little is known about the synaptic connectivity scheme of different GPe neurons toward both motor-suppressing pathways, as well as how opposite changes in GPe neuronal activity relate to locomotion inhibition. Here, we optogenetically dissect the input organizations of prototypic and arkypallidal neurons and further define the circuit mechanism and behavioral outcome associated with activation of the indirect or hyperdirect pathways. This work reveals that arkypallidal neurons are part of a novel disynaptic feedback loop differentially recruited by the indirect or hyperdirect pathways and that broadcasts inhibitory control onto locomotion only when arkypallidal neurons increase their activity.

INTRODUCTION

Action execution requires the selection of appropriate motor programs while suppressing unwanted ones and this function is crucial for interaction and survival in an ever-changing environment. The basal ganglia (BG) circuits form highly conserved neuronal networks in vertebrates[1], and their activity is critical to gate the motor components and adjust the vigor of goal-directed actions while also being involved in many parallel brain functions including motivation, decision making, and associative learning[2–8]. Rate-coding models of BG functional organization predict that actions are selected or inhibited depending on the level of activity of their GABAergic outputs[9,10]. Indeed, the tonic activity of BG output nuclei exerts sustained inhibition onto thalamus and brainstem motor programs[5,11–14]. Accordingly, action facilitation requires a disinhibition mechanism induced by the suppression of BG output activity, a condition fulfilled when the so-called direct pathway—the projections from D1-expressing striatal neurons (D1-SPNs) to BG outputs—is activated[5,15–18]. In contrast, action inhibition has been associated with increased BG output activity and two BG network mechanisms have been considered so far to underlie such an effect. The first requires activation of the indirect pathway[5,15]. Indeed, activation of this polysynaptic route—that includes projections from D2-expressing striatal neurons (D2-SPNs), the external globus pallidus (GPe), and subthalamic nucleus (STN) to BG outputs—leads to an increase in BG output firing and has thus been considered as a "no-go" signal. The second one is dependent upon the activation of the hyperdirect pathway, which provides a fast route linking the cortex to BG outputs through the STN, and it has been associated with a "stop" signal[16,19].

Although helpful in providing a general framework to apprehend BG function and dysfunction, BG models have been challenged by many functional and structural findings[20]. In particular, one limiting aspect is the key contribution of the GPe in these circuits, which has been previously overlooked[21]. Indeed, the GPe is a hub nucleus at the interface of the indirect and hyperdirect pathways integrating a large amount of striatal D2-SPN and STN inputs, whereas its long-range GABAergic projections target the whole BG to control and orchestrate BG neuronal activity[22–33]. Because D2-SPN and STN inputs are of opposite nature at the level of the GPe (i.e., inhibitory for D2-SPN and excitatory for STN inputs), it is not clear how different modulation of GPe activity can lead to the same inhibitory effect on motor action. In addition, whereas classic models assume the GPe to be composed of only one cell population projecting only to the STN, recent findings have described an overall dichotomous organization of GPe neurons at the molecular, structural, and functional levels[23,33,34]. Prototypic GPe neurons represent the main population with ~70% of all GPe neurons and have the "classic" features of GPe neurons: tonic activity and long-range projections to the substantia nigra pars reticulata (SNR) and the STN[23,28–30].

Please cite this article in press as: Aristieta et al., A Disynaptic Circuit in the Globus Pallidus Controls Locomotion Inhibition, Current Biology (2020), https://doi.org/10.1016/j.cub.2020.11.019

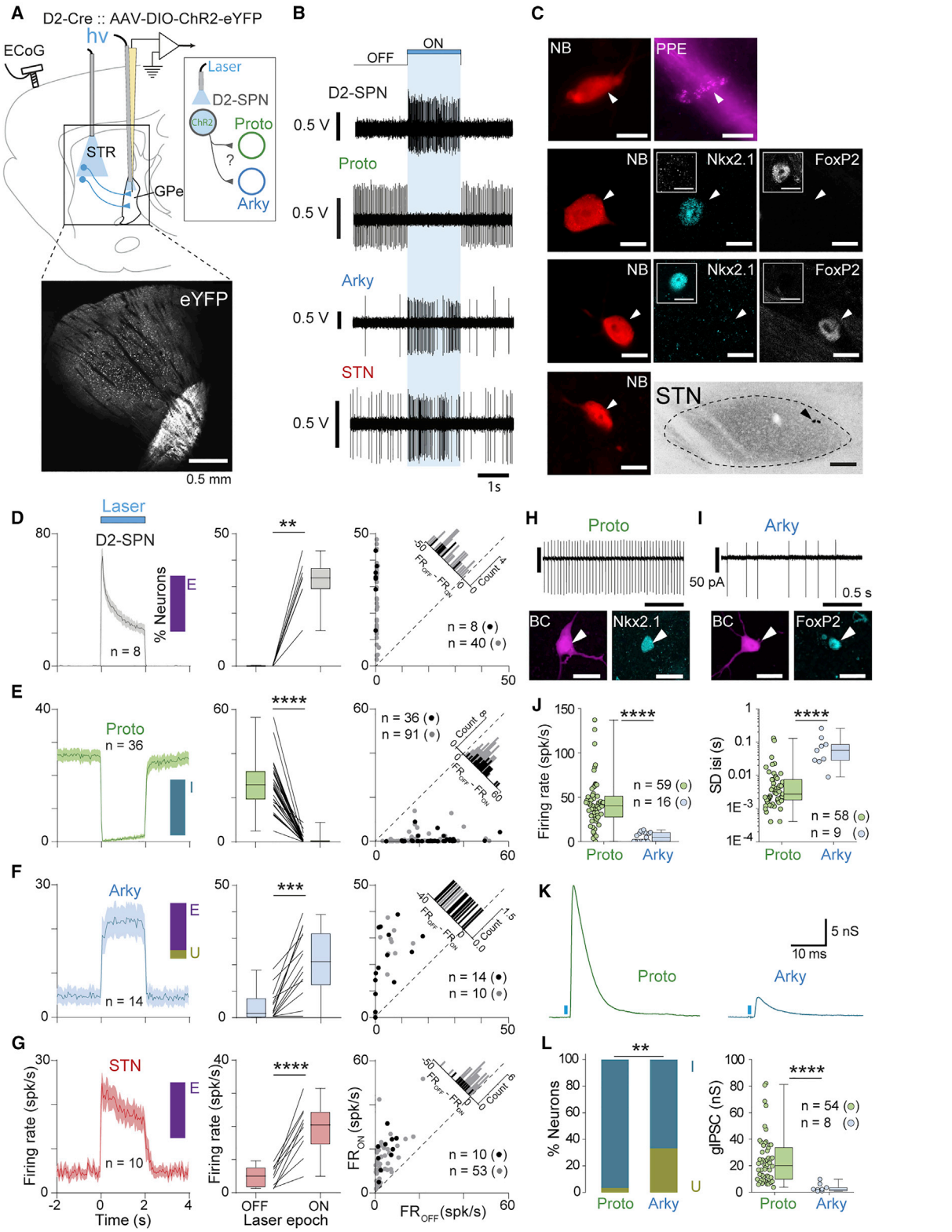

Figure 1. Opto-activation of D2-SPNs Induced Opposing Effects on Prototypic and Arkypallidal Neurons

(A) Schematic of the experimental design in D2-Cre mice injected with AAV-DIO-ChR2-eYFP in the striatum (STR). The epifluorescent image illustrates the ChR2-eYFP expression in D2-SPNs with dense axonal projections to the GPe (the scale bar represents 0.5 mm).

(B) Representative examples of D2-SPN opto-excitation on the *in vivo* firing activity of identified D2-SPN, prototypic, arkypallidal, and STN neurons.

(legend continued on next page)

Please cite this article in press as: Aristieta et al., A Disynaptic Circuit in the Globus Pallidus Controls Locomotion Inhibition, Current Biology (2020), https://doi.org/10.1016/j.cub.2020.11.019

On the contrary, arkypallidal neurons represent a unique cell population reaching ~30% of all GPe cells and project massively only to the striatum[23]. In addition, in rats performing a stop-signal task, arkypallidal neuron firing can efficiently suppress ongoing striatal activity[25], suggesting the existence of a novel "cancel" pathway not previously accounted for by BG models and that provides the animal with a mechanism to interrupt imminent actions independent of the traditional indirect no-go pathway. This functional GPe organization raises important questions regarding how both cell populations integrate striatal D2-SPN and STN inputs. In this work, we used optogenetic approaches combined with *in vivo* and *ex vivo* recordings to dissect the functional connectome of D2-SPN and STN inputs onto identified arkypallidal and prototypic GPe neurons. We also assessed the functional contribution of both pathways in the context of locomotion control. Our results show the existence of a novel disynaptic pathway differentially recruited by the indirect and hyperdirect pathways that can efficiently control animal locomotion. These findings place the GPe in a hub position to powerfully switch ongoing actions from execution to inhibition.

RESULTS

Identification of Prototypic and Arkypallidal Neurons in D2-Cre and Vglut2-Cre Transgenic Mice

Prototypic and arkypallidal neurons have been described to present different *in vivo* and *ex vivo* electrical properties in both wild-type animals[25,33,34] and transgenic mice[30,35,36]. To confirm the distinct electrophysiological properties of the two identified GPe cell populations in transgenic D2-Cre and Vglut2-Cre mice, we recorded GPe neuronal activity *in vivo* and *ex vivo* and labeled cells with neurobiotin/biocytin for post hoc immunochemical identification of the recorded neurons (Figure S1). Cell-type classification into prototypic and arkypallidal neurons was based on the differential expression profile of specific transcription factors: prototypic neurons expressed the transcription factor homeobox protein Nkx-2.1 (Figure S1A) whereas arkypallidal neurons were immunopositive for forkhead-box P2 (FoxP2) (Figure S1B). The electrical activities of Nkx-2.1+ prototypic and FoxP2+ arkypallidal neurons were noticeably different both *in vivo* and *ex vivo*, in agreement with previous reports[33,34]. In particular, prototypic neurons had a significantly higher firing rate and were more regular (Figures S1E–S1J; Table S2) than arkypallidal neurons, which often had an irregular activity including a long epoch of silence, especially *ex vivo* (Figures S1E–S1J; Table S2). These distinct electrical properties were also used to build a larger database that includes all recorded but unlabeled putative prototypic and arkypallidal GPe cell types (Figures S1E–S1J). Comparisons of the data collected from putative GPe neurons were in agreement with the data obtained from identified cells (Figures S1E–S1J; Table S2).

Striatopallidal Inputs Differentially Impact onto Prototypic and Arkypallidal Neurons

The striatopallidal (i.e., D2-SPN) projections represent the principal GABAergic inputs to the GPe[22,37]. To investigate the functional connectome of striatopallidal inputs onto prototypic and arkypallidal neurons, we used D2-Cre mice injected with an adeno-associated virus (AAV) containing a floxed channelrhodopsin (AAV-DIO-ChR2) in the striatum (Figure 1A). We first validated this D2-Cre::AAV-DIO-ChR2 opto-excitatory approach by testing the expression of preproenkephalin in a sample of opto-tagged striatal neurons (Figures 1B and 1C). Application of 2-s-long blue light pulses induced a strong excitation in all identified D2-SPNs (Figure 1D). We then studied the downstream impact of such D2-SPN photo-activation on the spontaneous firing activity of identified GPe neurons *in vivo*. We found that prototypic neurons were profoundly inhibited during D2-SPN opto-excitation (Figures 1B and 1E) whereas arkypallidal (Figures 1B and 1F) and STN (Figures 1B and 1G) neurons were both robustly excited. To further dissect the functional dynamics of D2-SPN inputs with finer temporal resolution, we then applied opto-stimulation using light pulses of 10-ms duration (Figure S2A). These shorter stimulations evoked more realistic firing activity in D2-SPN neurons, yet reproduced the core findings obtained with longer stimulation protocols. Indeed, all prototypic neurons exhibited a fast inhibitory response (mean of 8.7 ± 0.4 ms) hinting at a direct monosynaptic connectivity whereas the recovery of the baseline firing rate was relatively slow (Figures S2B–S2D; Table S2). Interestingly, the excitatory responses induced in arkypallidal and STN neurons parallel nicely the time course of prototypic inhibition (Figures S2B–S2D; Table S2). Importantly, this opposition of firing rate responses, observed both upon long and short D2-SPN opto-excitations between prototypic versus arkypallidal and STN neurons, was identical in our larger dataset including all recorded

(C) Recorded neurons were juxtacellularly labeled with neurobiotin (NB) and then tested for the expression of specific molecular markers: D2-SPNs are preproenkephalin positive (PPE); prototypic and arkypallidal GPe neurons express Nkx2.1 and FoxP2, respectively (the scale bars represent 10 μm in the confocal images and 0.1 mm in the STN image).

(D–G) Population peri-stimulus time histograms (PSTHs) (left; bin size, 50 ms), firing rate changes (middle), and scatterplot responses (right) during OFF versus ON D2-SPN opto-excitation for all the recorded and juxtacellularly labeled (black dots) or putative (gray dots) D2-SPN (D), prototypic (E), arkypallidal (F), and STN neurons (G). The inset bar plots represent the percentage of neurons excited (E), inhibited (I), and unaffected (U) by the light stimulation.

(H and I) Typical example of biocytin-filled prototypic (Nkx2.1+) and arkypallidal neurons (FoxP2+) with their corresponding activity recorded in cell-attached patch-clamp recordings (the scale bars represent 10 μm).

(J) Box-and-whisker plots depicting average firing rate (FR) and the standard deviation of the interspike interval (SDisi) of prototypic (green) and arkypallidal neurons (blue).

(K) Representative examples of inhibitory post-synaptic currents (IPSCs) recorded in prototypic and arkypallidal neurons.

(L) Bar graph representing the proportion of D2-SPN-recipient prototypic and arkypallidal neurons and corresponding box-and-whisker plot of average IPSC conductance for each cell population.

Group data represent mean ± SEM; box-and-whisker plots indicate median, first and third quartile, and min and max values. $^{**}p < 0.01$, $^{***}p < 0.001$, $^{****}p < 0.0001$.

See also Figures S1–S4 and Tables S1 and S2 for more details and statistical information.

Please cite this article in press as: Aristieta et al., A Disynaptic Circuit in the Globus Pallidus Controls Locomotion Inhibition, Current Biology (2020), https://doi.org/10.1016/j.cub.2020.11.019

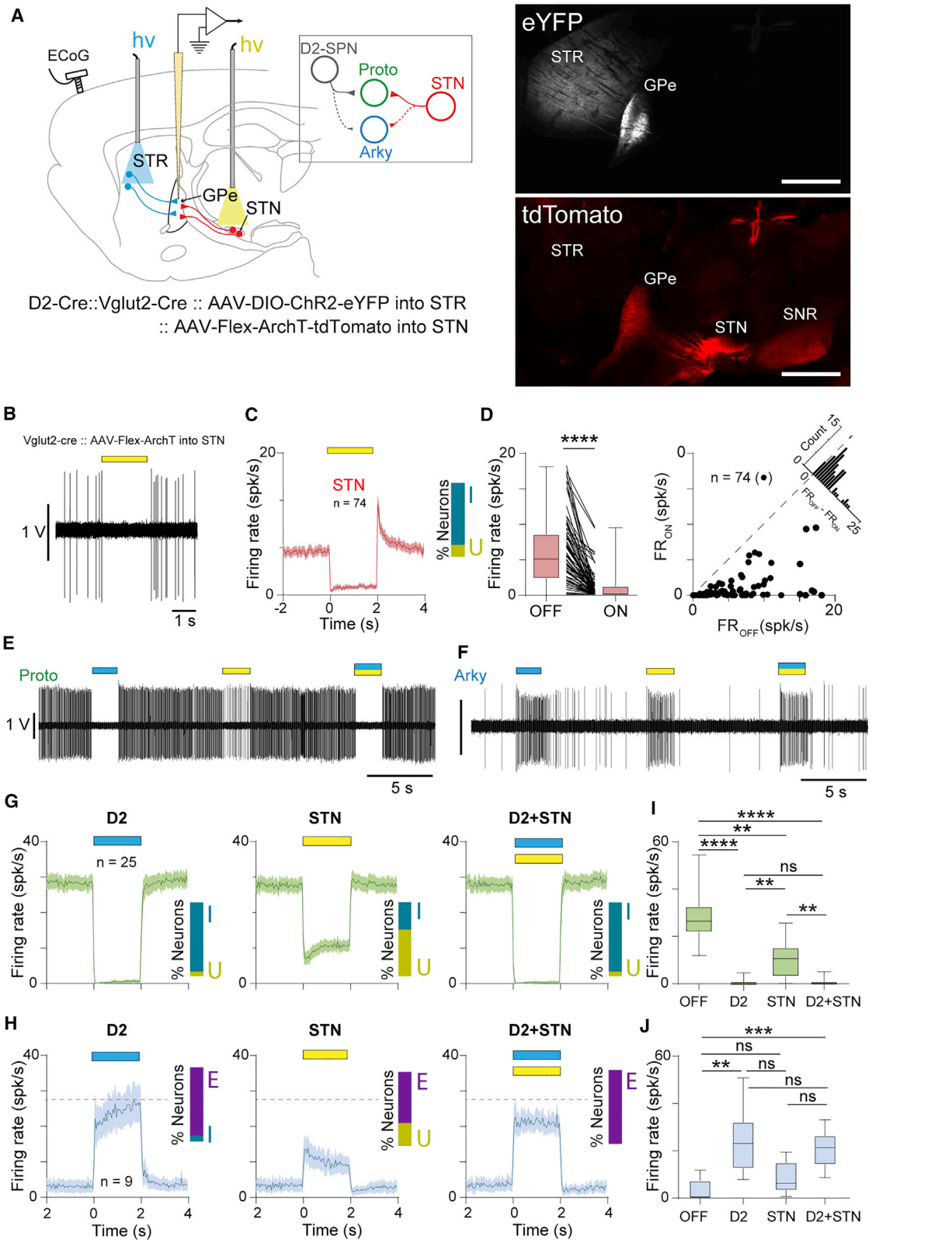

Figure 2. Opto-inhibition of STN Neurons Increased the Firing Rate of Arkypallidal Neurons *In Vivo*

(A) Schematic of the experiments in double-D2-Cre::Vglut2-Cre mice injected with AAV-DIO-ChR2-eYFP in the STR and AAV-Flex-ArchT3-mCherry in the STN (the scale bars represent 2 mm).

(legend continued on next page)

Please cite this article in press as: Aristieta et al., A Disynaptic Circuit in the Globus Pallidus Controls Locomotion Inhibition, Current Biology (2020), https://doi.org/10.1016/j.cub.2020.11.019

putative GPe cell populations (Figure S3; Table S2). This confirms that these stereotypical responses are robust features underlying the functional dynamics that exist between these different cell populations. To further investigate the synaptic mechanism leading to such opposition of *in vivo* firing between GPe neurons, we next performed *ex vivo* patch-clamp recordings on prototypic and arkypallidal neurons (Figures 1H–1J; Table S1) in D2-Cre::AAV-DIO-ChR2 and D2-Cre::Ai32 mice (Figures S4A and S4B). This latter mouse line unequivocally ensures that all D2-SPNs are expressing ChR2, thus ruling out the possibility that differential neuronal responses in the GPe are caused by improper viral vector expression. Characterization of D2-SPN inputs using these two optogenetic strategies reveals a similar proportion of input-recipient prototypic and arkypallidal neurons (Figures S4C and S4D; Table S2), and therefore data obtained from D2-Cre::AAV-ChR2 and D2-Cre::Ai32 were pooled together for both identified (Figures 1K and 1L) and putative (Figures S4E and S4F) prototypic and arkypallidal neurons, respectively. We found that opto-excitation of D2-SPN inputs with a light pulse of 1 ms reliably evoked inhibitory post-synaptic current (eIPSC) in nearly all prototypic neurons whereas a significant fraction of arkypallidal neurons (~30%) did not receive any inhibitory inputs from D2-SPNs (Figure 1L). In addition, the eIPSCs were on average 85% smaller in magnitude in arkypallidal than in prototypic neurons (Figures 1K and 1L; Table S1). These properties were also confirmed when considering all putative GPe neurons recorded (Figures S4E and S4F; Table S2). Altogether, these results support the view that D2-SPN inputs differentially impact onto prototypic and arkypallidal neurons, with arkypallidal neurons receiving weaker and less numerous projections from D2-SPNs as compared to prototypic neurons. Because prototypic neurons efficiently control BG network dynamics[26] through their widespread local axon collaterals (i.e., intra GPe) and distal projections[23,27–29,38,39], their preferential inhibition by D2-SPNs will therefore cause a disinhibition in arkypallidal and STN neurons as revealed by their increased firing *in vivo*.

Opto-inhibition of STN Neurons Increases the Firing Rate of Arkypallidal Neurons *In Vivo*

Although disinhibition mechanisms from prototypic neurons have been shown to account for the increased firing observed in the STN following GPe opto-inhibition[26,40], the increased firing of arkypallidal neurons upon D2-SPN opto-excitation could alternatively be driven by the concurrent increase of STN firing that represents the main excitatory input to the GPe[41,42]. To better dissect the network mechanism and test whether a disinhibition from prototypic neurons or a direct excitation from the STN is leading to an increased firing of arkypallidal neurons, we generated a D2-Cre::Vglut2-Cre double-transgenic mouse line to opto-manipulate D2-SPNs and STN neurons independently in the same animal. We injected these mice with AAV-DIO-ChR2 in the striatum—for opto-excitation of D2-SPNs—and AAV-flex-ArchT into the STN—for opto-inhibition (Figure 2A). The validation of ArchT-mediated photo-inhibition of STN neurons (Figure 2B) shows that most STN neurons were indeed profoundly inhibited by ArchT activation (Figures 2C and 2D; Table S1). We next tested the consequences of D2-SPN photo-excitation versus STN photo-inhibition alone, or their concurrent effect on prototypic and arkypallidal neuronal activity *in vivo* (Figures 2E and 2F). As expected from our previous experiments, opto-excitation of D2-SPN inputs induced opposite responses in the two GPe cell populations, with prototypic neurons showing an inhibition (Figures 2G and 2I) and arkypallidal neurons increasing their activity (Figures 2H and 2J). Opto-inhibition of STN inputs also led to opposite responses between the two GPe cell types, with prototypic neurons decreasing their firing activity on average and arkypallidal neurons showing an overall increased response (Figures 2I and 2J; Table S1). Interestingly, the suppression of the STN tonic excitatory drive seemed to affect the tonic firing of a small proportion of prototypic neurons whereas the arkypallidal response was a mirror image in the opposite direction. This highlights the likely contribution of collateral inhibition from prototypic neurons to shape the activity of arkypallidal neurons. The concurrent excitation of D2-SPN and inhibition of STN inputs did not suppress the excitatory response of arkypallidal neurons but only slightly decreased it (Figures 2I and 2J; Table S1). Altogether, these results indicate that the response of arkypallidal neurons to D2-SPN inputs is principally driven by a disinhibition from prototypic neurons, with only a small contribution from the direct STN excitatory drive.

STN Inputs Preferentially Excite Prototypic Neurons, Causing a Disynaptic Inhibition in Arkypallidal Neurons

To next define the functional connectome of STN inputs onto GPe neurons, we used Vglut2-Cre mice injected with AAV-DIO-ChR2 in the STN (Figure 3A). Our *in vivo* electrophysiological recordings coupled with juxtacellular labeling confirmed the efficient opto-excitation of STN neurons in these mice, using either 2-s- (Figures 3B and 3C) or 10-ms-long laser pulses (Figures S5A and S5B). We then investigated the impact of STN inputs in the GPe *in vivo*. We found that all prototypic neurons were strongly excited by STN afferents (Figures 3B and 3D–3F; Table S1) with fast latency (mean of 5.2 ± 0.6 ms) as best measured with the 10-ms laser stimulation protocols (Figure S5). On the other hand, most arkypallidal neurons had a strong inhibition of their firing in response to STN inputs

(B) Representative opto-inhibition example of an STN neuron recorded *in vivo*.
(C) Population PSTH (bin size, 50 ms) of STN neuron opto-inhibition.
(D) Box-and-whisker plot (left) and scatterplot distribution (right) of STN neurons firing during OFF versus ON opto-inhibition.
(E and F) Representative firing activity examples of prototypic (E) or arkypallidal neurons (F) illustrating the effect of D2-SPN opto-activation (blue bar), STN opto-inhibition (yellow bar), and D2-SPN opto-activation + STN opto-inhibition (blue and yellow bars).
(G and H) Population PSTHs (bin size, 50 ms) of D2-SPN opto-activation (left), STN opto-inhibition (middle), and D2-SPN opto-activation + STN opto-inhibition (right) effects on prototypic (G) and arkypallidal neurons (H).
(I and J) Firing rate changes of prototypic (I) or arkypallidal neurons (J) during OFF versus ON D2-SPN opto-activation (D2), STN opto-inhibition (STN), and D2-SPN opto-activation + STN opto-inhibition (D2+STN).
The inset bar plots in (C), (G), and (H) represent the percentage of neurons excited (E), inhibited (I), and unaffected (U) by the light stimulation. Group data represent mean ± SEM; box-and-whisker plots indicate median, first and third quartile, and min and max values. $^{**}p < 0.01$, $^{***}p < 0.001$, $^{****}p < 0.0001$; ns, not significant. See Table S1 for more details and statistical information.

Please cite this article in press as: Aristieta et al., A Disynaptic Circuit in the Globus Pallidus Controls Locomotion Inhibition, Current Biology (2020), https://doi.org/10.1016/j.cub.2020.11.019

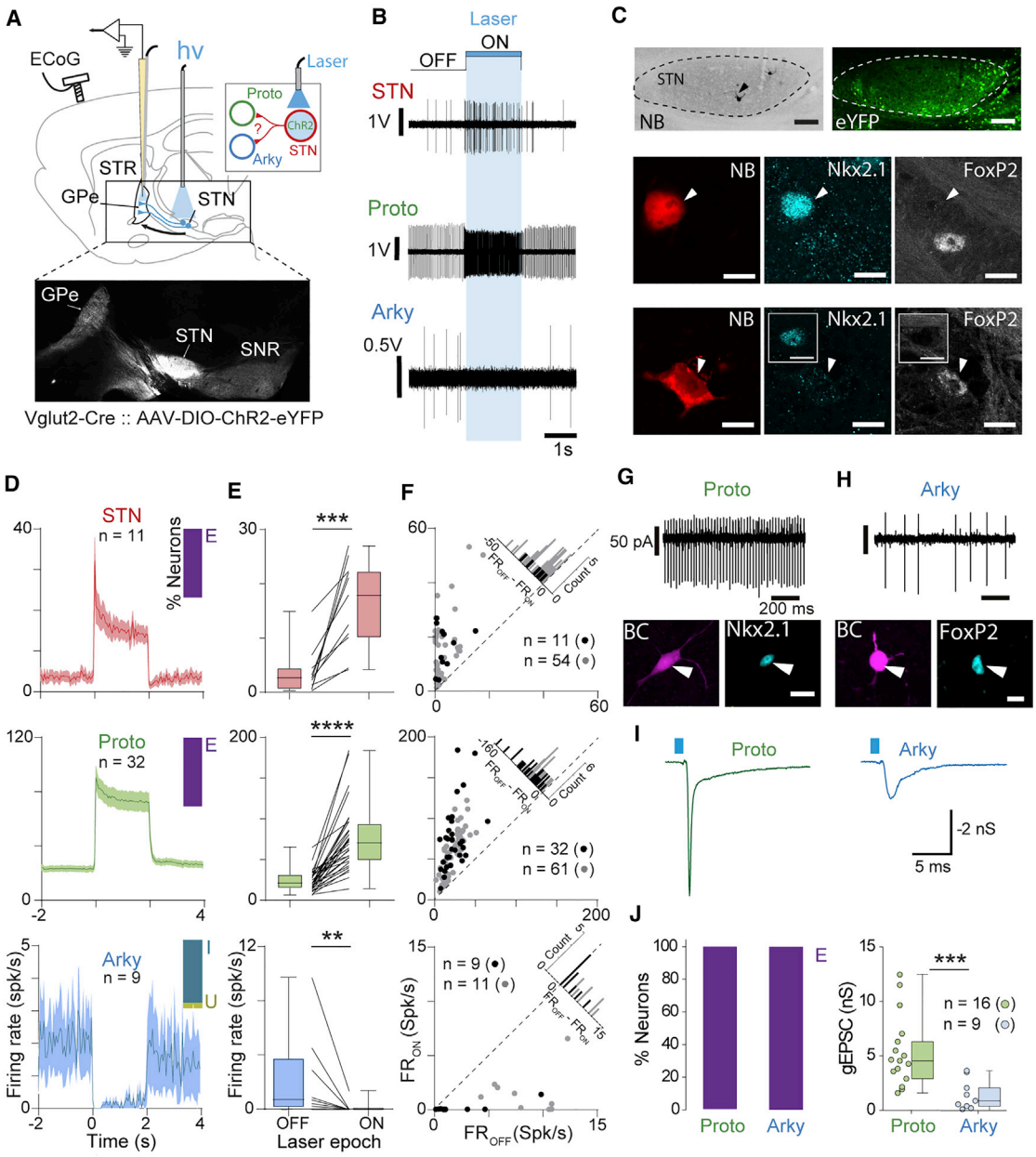

Figure 3. Opto-activation of STN Neurons Induced Opposing Effects on Prototypic and Arkypallidal Neurons

(A) Schematic of the experimental design in Vglut2-Cre mice injected with AAV-DIO-ChR2-eYFP in the STN and recorded in the GPe. The epifluorescent image shows ChR2-eYFP expression in the STN and its axonal projections to the GPe and SNR.

(B) Representative examples of *in vivo* juxtacellularly labeled STN, prototypic, and arkypallidal neurons showing the effect of STN opto-activation on their firing activities.

(C) Microphotographs of STN (the scale bars represent 0.1 mm), prototypic, and arkypallidal neurons juxtacellularly labeled *in vivo* with neurobiotin (arrows) and tested for the labeling of Nkx2.1 and FoxP2 (the scale bars in the confocal images represent 10 μm).

(D) Population PSTHs (bin size, 50 ms) of all the *in vivo* juxtacellularly labeled STN (top), prototypic (middle), and arkypallidal neurons (bottom) during STN opto-activation. The inset bar plots represent the percentage of neurons excited (E), inhibited (I), and unaffected (U) by the light stimulation.

(E) Box-and-whisker plots of the firing rate changes of all the juxtacellularly labeled STN (top), prototypic (middle), and arkypallidal neurons (bottom) during laser OFF versus ON STN opto-activation.

(F) Scatterplot distributions of the juxtacellularly labeled (black dots) and putative (gray dots) STN (top), prototypic (middle), and arkypallidal neurons (bottom).

(G and H) Biocytin-filled prototypic (Nkx2.1+) and arkypallidal neurons (FoxP2+) with their corresponding activity recorded in cell-attached patch-clamp recordings.

(I) Representative examples of excitatory post-synaptic currents (EPSCs) recorded in prototypic and arkypallidal neurons.

(legend continued on next page)

Please cite this article in press as: Aristieta et al., A Disynaptic Circuit in the Globus Pallidus Controls Locomotion Inhibition, Current Biology (2020), https://doi.org/10.1016/j.cub.2020.11.019

(Figures 3B and 3D–3F; Table S1), which could last up to 50 ms when using short laser pulses (Figure S5; Table S2). These results were identical when considering a larger dataset that included all the putative GPe neurons (Figure S6; Table S2). Such differential firing responses toward STN inputs is consistent with our previous findings in rats in which opto-excitation of STN neurons led to quick excitation in prototypic neurons but inhibition in arkypallidal neurons[26]. Thus, similar to D2-SPN inputs, activation of STN glutamatergic afferents impacts preferentially onto prototypic and not arkypallidal neurons. The strong excitatory response evoked in prototypic neurons is associated with an inhibition of arkypallidal neurons, which was likely caused by disynaptic inhibition from prototypic axon collaterals. To investigate the synaptic origin of this *in vivo* differential GPe neuronal response toward STN inputs, we next performed GPe patch-clamp recordings in acute brain slices of Vglut2-Cre mice injected with an AAV-DIO-ChR2 virus in the STN (Figures 3G and 3H). Interestingly, all identified prototypic and arkypallidal neurons that were recorded exhibited excitatory post-synaptic currents (EPSCs) evoked by opto-activation of STN synaptic terminals in the GPe (Figures 3I and 3J). However, similar to inhibitory inputs coming from D2-SPNs, STN inputs were 74% smaller in arkypallidal than in prototypic neurons (Figure 3J; Table S1). The same trend was also observed on a larger sample of unlabeled neurons (Figure S7; Table S2). In conclusion, our data support the view that the functional connectome of STN inputs preferentially excites prototypic neurons that likely cause, in return, a powerful disynaptic inhibition in arkypallidal neurons. This result highlights the possibility that collateral inhibition from prototypic neurons is overriding a direct excitation of the STN onto arkypallidal neurons and suggests that the activity of arkypallidal neurons is tightly controlled by prototypic neurons.

With this in mind, we next tested whether the disynaptic inhibition exerted by prototypic neurons onto arkypallidal neurons could be suppressed by external inputs, thus unmasking the direct excitation of STN inputs onto arkypallidal neurons. To do so, we studied the effect of concurrent opto-excitation of D2-SPN inputs (to suppress the activity of prototypic neurons) and STN inputs (to drive excitation) on the activity of arkypallidal neurons in D2-Cre::Vglut2-Cre mice injected with the AAV-DIO-ChR2 virus in both the striatum and STN (Figures 4A and 4B). As described before, photo-activation of D2-SPN inputs increased the firing of arkypallidal neurons (Figure 4C) whereas photo-activation of the STN induced an overall inhibition of their activity (Figure 4D), and these results were similar for both long (i.e., 2 s) and short (i.e., 10 ms) laser stimulation protocols. Interestingly, though, the concurrent opto-activation of both D2-SPN and STN inputs induced a stronger excitation in arkypallidal neurons than D2-SPN inputs alone (Figure 4E), although this effect was not statistically significant in our sample size (Figures 4F and 4G; Table S1). We have previously shown that the excitatory response of arkypallidal neurons induced by D2-SPN inputs is mostly caused by a disinhibition mechanism with only a small contribution of the STN direct excitation (see Figure 2). We thus confirm here that STN inputs are capable of directly exciting arkypallidal neurons but only when the disynaptic inhibition normally exerted by prototypic neurons is removed. This suggests a rather complex mechanism by which striatal D2-SPN inputs could gate the integration of STN information in the GPe and determine which cell population in the GPe will be excited by STN inputs.

Prototypic Neurons Control the Activity of Arkypallidal Neurons through Axon Collateral Inhibition

GPe neurons, especially prototypic neurons, have dense axon collaterals[23,27,39,43,44], yet characterization of lateral inhibition between prototypic and arkypallidal neurons has never been investigated functionally. To first explore whether prototypic neuron collaterals could efficiently inhibit arkypallidal neurons, we injected an AAV-DIO-ChR2 virus into the GPe of Nkx2.1-Cre mice that provides genetic access to the prototypic population based on the selective expression of Nkx2.1 in prototypic neurons[33,34]. The expression of ChR2 as reported by the visualization of the reported protein mCherry was accordingly restricted to prototypic neurons (Figures 5A and 5B). Opto-excitation of prototypic neurons in a cell-attached configuration produced a strong and sustained increase in their firing (Figures 5C and 5E; Table S1), whereas it induced a potent inhibition of the firing activity of all recorded arkypallidal neurons (Figures 5D and 5F; Table S1). Light-evoked IPSCs were detected both in arkypallidal and prototypic neurons. Although our sample size did not yield a significant difference, our data trended toward larger IPSCs in arkypallidal neurons (Figure 5G; Table S1). These results support the existence of functional collateral connections between prototypic and arkypallidal neurons, as previously suggested by anatomical studies[23]. We then investigated whether these collateral connections were reciprocal with arkypallidal neurons inhibiting prototypic neurons. To do so, we injected an AAV-DIO-ChR2 virus into the GPe of FoxP2-Cre mice (Figure 6A) that enabled specific expression of ChR2 in arkypallidal neurons (Figure 6B) and recorded GPe neurons in acute brain slices. Photo-activation of arkypallidal neurons efficiently increased the firing in all recorded arkypallidal neurons, thus validating this approach (Figures 6C and 6E; Table S1); however, this strategy did not produce any inhibitory responses in prototypic neurons (Figures 6D and 6F; Table S1). To confirm that the absence of inhibitory responses was genuinely caused by a lack of connections rather than an artifactual disconnection produced by the slicing procedure, we next performed *in vivo* single-unit recordings in anesthetized FoxP2-Cre mice similarly injected with an AAV-DIO-ChR2 virus in the GPe (Figure 6G). Light activation also led to an increased firing rate of arkypallidal neurons recorded *in vivo* (Figure 6H), but this excitation had no effect on the average output activity of GPe prototypic neurons (Figure 6I; Table S1). Looking further into the effects at the individual neuron level, we found that photo-excitation of arkypallidal neurons produces for the most part no effect on prototypic neurons whereas a minority was either excited or inhibited (Figure 6I), supporting the conclusion

(J) Bar graphs representing the proportion of STN-recipient prototypic and arkypallidal neurons and corresponding box-and-whisker plots of average EPSC conductance for each cell population.

Group data represent mean ± SEM; box-and-whisker plots indicate median, first and third quartile, and min and max values. $^{**}p < 0.01$, $^{***}p < 0.001$, $^{****}p < 0.0001$.

See also Figures S5–S7 and Tables S1 and S2 for more details and statistical information.

Please cite this article in press as: Aristieta et al., A Disynaptic Circuit in the Globus Pallidus Controls Locomotion Inhibition, Current Biology (2020), https://doi.org/10.1016/j.cub.2020.11.019

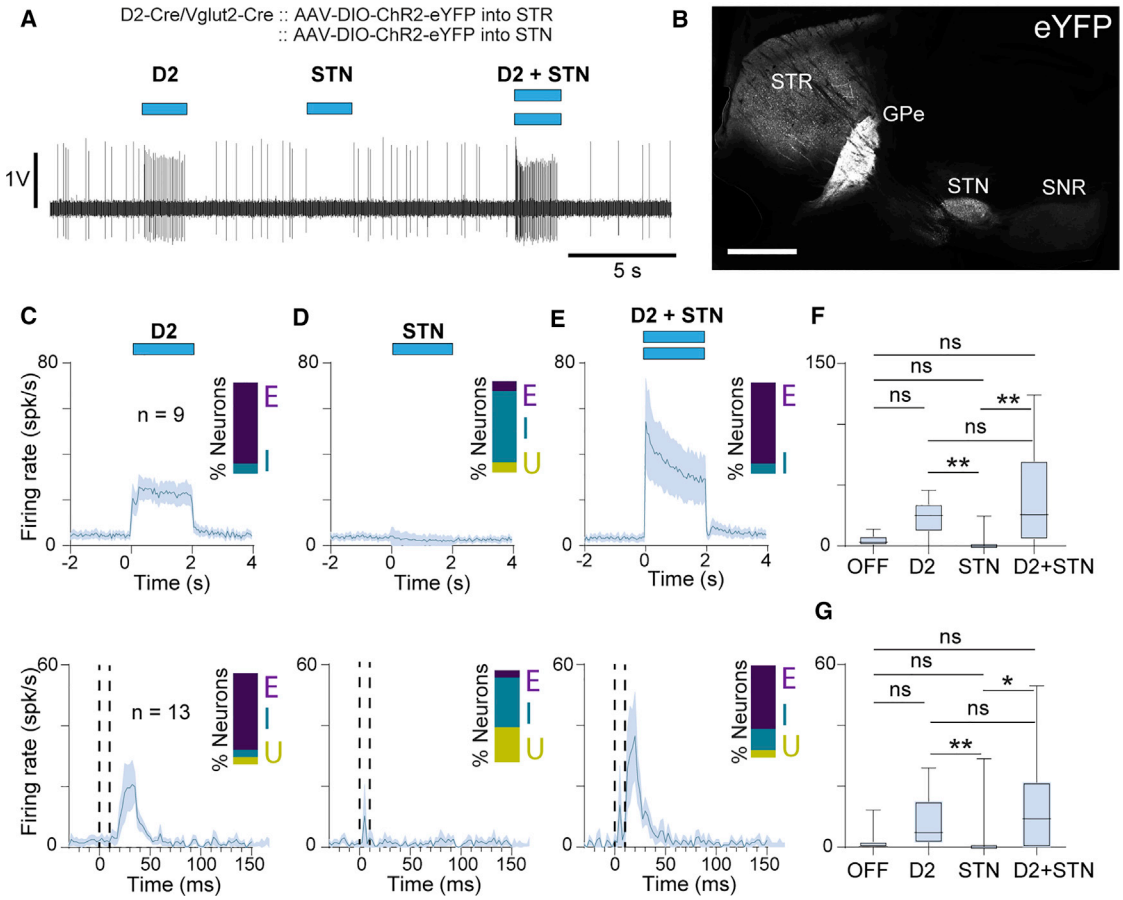

Figure 4. The *In Vivo* Integration of STN Inputs in Arkypallidal Neurons Is Gated by the Presence of D2-SPN Inputs

(A) Representative single-unit recording showing the effect of D2-SPN (D2 stim), STN (STN stim), and D2-SPN + STN (D2 stim + STN stim) opto-activation (2-s blue light pulses) on the firing activity of one arkypallidal neuron.

(B) Epifluorescent image illustrating the ChR2-eYFP expression in D2-SPN and STN neurons with dense axonal projections to the GPe (the scale bar represents 1 mm).

(C–E) Population PSTHs of arkypallidal neurons calculated during a 2-s long (top; bin size, 50 ms) or a 10-ms short (bottom; bin size, 2.5 ms) opto-activation of D2-SPN (C), STN (D), and D2-SPN + STN (E) inputs. The inset bar plots represent the percentage of neurons excited (E), inhibited (I), and unaffected (U) by the light stimulation.

(F and G) Average firing rate changes in arkypallidal neurons calculated during a 2-s long (F) or a 10-ms short (G) OFF versus ON opto-activation of D2-SPN (D2), STN, and D2-SPN + STN (D2+STN) inputs.

Group data represent mean ± SEM; box-and-whisker plots indicate median, first and third quartile, and min and max values. *$p < 0.05$, **$p < 0.01$; ns, not significant. See also Table S1 for more details and statistical information.

of a rather weak functional connection between arkypallidal and most prototypic neurons. Altogether, our results are in line with the small proportion of arkypallidal neurons (~30%) compared to the total number of GPe neurons[33] and the small number of synaptic terminals made by these neurons within the GPe[23]. This dataset thus suggests the existence of a unilateral connectivity from prototypic to arkypallidal neurons that provides the anatomical architecture to promote a disynaptic circuit capable of turning the activity of arkypallidal neurons ON or OFF.

Excitation of Arkypallidal Neurons Is Sufficient for Locomotion Inhibition

Activation of both D2-SPNs (i.e., the indirect no-go pathway) and STN neurons (i.e., the hyperdirect stop pathway) has been considered to favor motor suppression. Considering the opposite impact that both pathway stimulations had on GPe prototypic and arkypallidal neuronal firing, we next tested whether the motor correlates caused by the photo-activation of both circuits were identical. To best detect an effect on movement inhibition, we recorded the locomotor activity of mice walking on a motorized treadmill and applied random 500-ms-duration optogenetic stimulations (Figure 7A). Both indirect (i.e., D2-SPNs) and hyperdirect (i.e., STN) pathways were photo-activated using bilateral injections of an AAV-DIO-ChR2 virus in the striatum (Figure 7B) or the STN (Figure 7C) of D2-Cre and Vglut2-Cre mice, respectively. Interestingly, we found that D2-SPN and STN stimulations caused different effects on locomotion. Indeed, activation of D2-SPNs induced a pronounced reduction in movement velocity (Figures 7E and 7I; Table S1) whereas the STN stimulation had no clear effect (Figures 7F and 7I; Table S1). Locomotion

Please cite this article in press as: Aristieta et al., A Disynaptic Circuit in the Globus Pallidus Controls Locomotion Inhibition, Current Biology (2020), https://doi.org/10.1016/j.cub.2020.11.019

CellPress
OPEN ACCESS

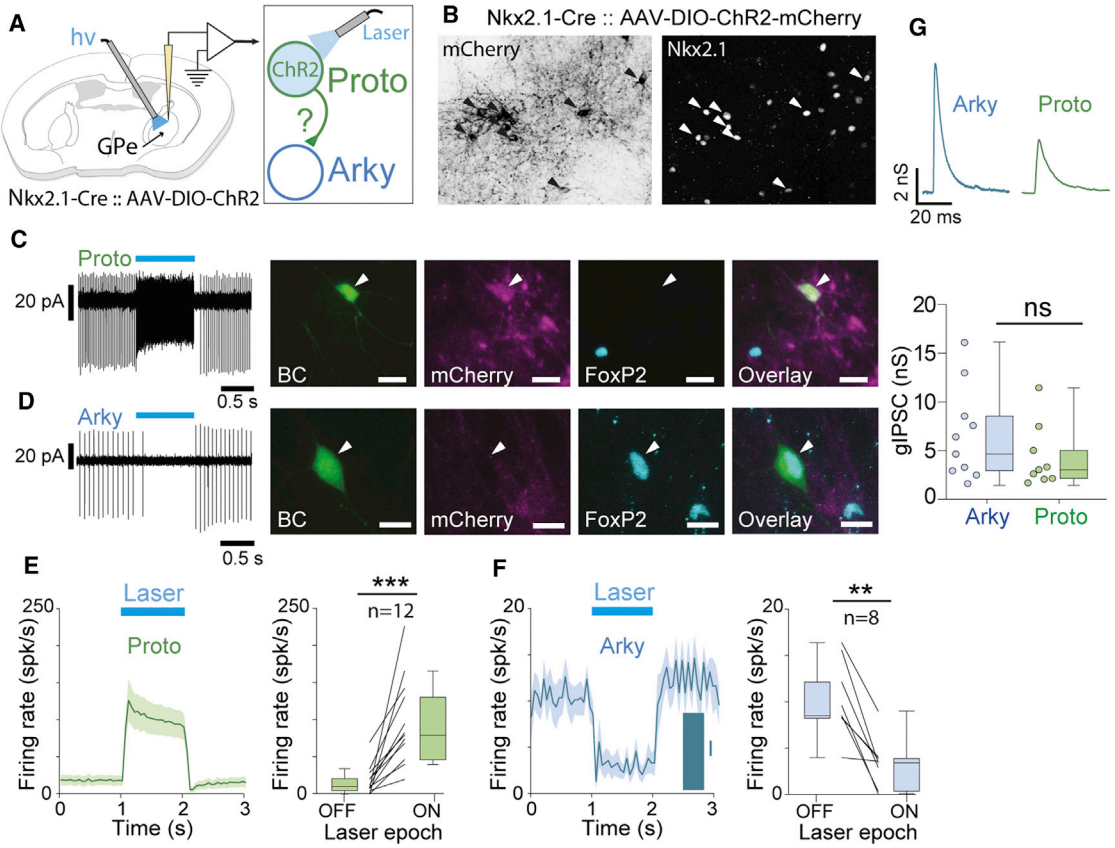

Figure 5. Prototypic Neuron Axon Collaterals Powerfully Inhibit Arkypallidal Neurons

(A) Schematic of the *ex vivo* experiments.

(B) Histological verification of the expression of AAV5-EF1a-DIO-ChR2(H134R)-mCherry in prototypic neurons (Nkx2.1+).

(C and D) Typical cell-attached activity of identified prototypic (C) and arkypallidal neurons (D) during OFF and ON epochs of laser stimulation with corresponding confocal images showing biocytin (BC), mCherry, and FoxP2 immuno-labeling signals (the scale bars represent 10 μm).

(E and F) Population PSTHs (left; bin size, 50 ms) and box-and-whisker plots (right) of prototypic (E) or arkypallidal neurons (F) firing during opto-activation.

(G) Representative examples (top) and box-and-whisker plots (bottom) representing GABAergic IPSC conductances recorded in arkypallidal (blue) and prototypic neurons (green).

Group data represent mean ± SEM; box-and-whisker plots indicate median, first and third quartile, and min and max values. **p < 0.01; ns, not significant. See also Table S1 for more details and statistical information.

experiments using mice injected with a control AAV-DIO-eYFP virus were also performed to test for the potential side effects induced by the light and the virus transduction associated with our optogenetic manipulations. These control optogenetic experiments showed no effect of light stimulation on the locomotor behavior (Figures 7H and 7I; Table S1). We next dissected whether the differential neuronal response observed in prototypic and arkypallidal neurons upon D2-SPN or STN stimulation could account for the differential effect on locomotion. Indeed, D2-SPN stimulation induced a pause in prototypic neurons firing and a strong disynaptic excitation in the arkypallidal population. Because arkypallidal neurons have been proposed to play an important role in movement cancellation[25], we hypothesized that the locomotion inhibition consequent to D2-SPN stimulations was mediated by the increased firing of arkypallidal neurons. To tease apart the specific functional contribution of prototypic versus arkypallidal neuronal response in locomotion inhibition, we used FoxP2-Cre mice, because these transgenic mice gave us the opportunity to test the contribution of the arkypallidal excitatory response without affecting the overall firing of prototypic neurons (see the results of Figure 6). Interestingly, we found that optogenetic excitation of arkypallidal FoxP2-expressing neurons reproduced a strong inhibition of locomotion (Figures 7D, 7G, and 7I; Table S1) and that this effect was significantly different in all FoxP2-Cre mice as compared to matched controlled experiments. Altogether, our results suggest that increased activity in arkypallidal neurons is sufficient to mediate locomotion inhibition.

DISCUSSION

Increased Arkypallidal Activity Causes Locomotion Inhibition

It has been proposed that arkypallidal neurons broadcast a "stop" signal (Figure 7J) to the striatum when an ongoing motor action has to be cancelled[25]. However, the direct contribution of arkypallidal neurons in motor inhibition has never been interrogated with cell-type-specific optogenetic stimulations before.

Please cite this article in press as: Aristieta et al., A Disynaptic Circuit in the Globus Pallidus Controls Locomotion Inhibition, Current Biology (2020), https://doi.org/10.1016/j.cub.2020.11.019

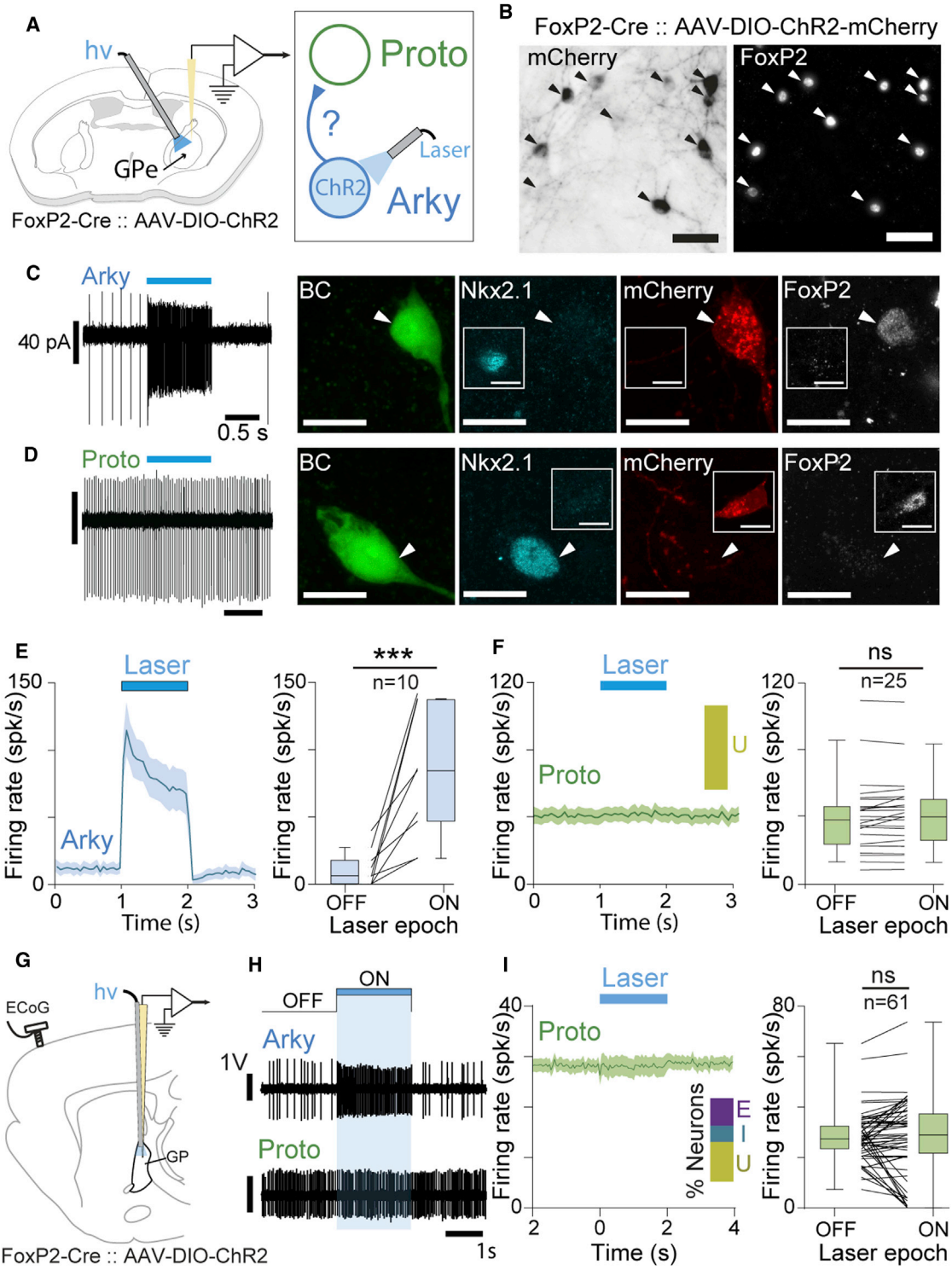

Figure 6. Arkypallidal Neurons Do Not Provide Functional Inhibition onto Prototypic GPe Neurons

(A) Schematic of the *ex vivo* experiments.

(B) Histological verification of the expression of AAV-DIO-ChR2-mCherry in arkypallidal neurons (FoxP2+).

(C and D) Typical cell-attached activity of identified arkypallidal (C) and prototypic neurons (D) during OFF and ON epochs of laser stimulation with corresponding confocal images of biocytin, Nkx2.1, mCherry, and FoxP2 immuno-labeling signals.

(E and F) Population PSTHs (right; bin size, 50 ms) and box-and-whisker plots (left) of arkypallidal (E) and prototypic neurons (F) firing during opto-activation.

(G) Schematic of the *in vivo* experiments.

(legend continued on next page)

Please cite this article in press as: Aristieta et al., A Disynaptic Circuit in the Globus Pallidus Controls Locomotion Inhibition, Current Biology (2020), https://doi.org/10.1016/j.cub.2020.11.019

Here, we show that opto-excitation of arkypallidal neurons causes a robust inhibition of ongoing locomotor activity. Interestingly, the light-driven activity increase of arkypallidal neurons does not modify the overall output activity of prototypic neurons. This suggests that the arkypallidal neuron-mediated inhibitory effect on movement is independent of any changes in prototypic neuronal activity and, thus, their downstream projection sites. Instead, we believe that locomotion inhibition is caused through a global suppression of "go-related" striatal activity mediated by the dense projections sent from arkypallidal neurons to the striatum[23,28] and that contact both striatal interneurons and SPN cell populations[23]. These results reveal an important function of arkypallidal neurons that is to control movement-related activity in the striatum either to suppress ongoing movement or to inhibit competitive actions. It is possible that action initiation is promoted by the inhibition of arkypallidal neurons. That being said, recordings of arkypallidal neurons during spontaneous movements have mainly shown increased activity in this cell population[33] but their low firing activity could make inhibition less detectable than in fast-firing neurons. Interestingly, it has been described that D1-SPNs send bridging collaterals to the GPe and that structural plasticity in these connections can rescue locomotor imbalance[37]. If the function of D1-SPNs in movement execution is principally driven by their direct inhibitory effect onto SNR activity[5,15], it is also possible that the bridging collaterals of D1-SPNs specifically suppress the activity of arkypallidal neurons. Thus, inhibiting the motor brake function exerted by arkypallidal neurons might facilitate action initiation and motor sequence execution. In support of this hypothesis, a recent work shows that the D1-SPN inhibitory inputs have a strong bias toward arkypallidal neurons[45].

D2-SPN Opto-activation Leads to a Disynaptic Excitation of Arkypallidal Neurons

In this study, we found that D2-SPN optogenetic activation induces locomotion inhibition, confirming the negative influence of the indirect pathway on movement execution[7,15,46–50]. In addition, our *ex vivo* electrophysiological recordings demonstrate that both prototypic and arkypallidal neurons receive inhibitory inputs from D2-SPNs, although the inhibitory currents detected in arkypallidal neurons are smaller than the ones in prototypic neurons. Such differential striatal innervation onto GPe neurons has already been reported but the molecular identity of GPe neurons was not defined[51,52]. By further dissecting how D2-SPN inputs impact onto different GPe neuronal populations *in vivo*, we revealed a cell-type-specific integration of these inputs. Indeed, prototypic neurons were almost fully silenced by D2-SPN inputs, whereas arkypallidal neurons were strongly excited. This opposition of response in arkypallidal neurons was caused by a disynaptic disinhibition mechanism involving axon collaterals from prototypic neurons. These results outline how a difference in the organization of synaptic inputs at the single-cell level measured *ex vivo* can give rise to opposite firing activities when cell populations are embedded into neuronal networks *in vivo*. In addition, our finding regarding D2-SPN stimulation leading to an increase in the activity of arkypallidal neurons raises new insights into the cellular mechanism causing movement inhibition consequent to the indirect pathway activation. In particular, we show that the excitation of arkypallidal neurons induces locomotion inhibition and that this effect is certainly due to the global suppression of striatal activity (Figure 7K). Although we show in this work that this mechanism is sufficient by itself to suppress locomotion, it is possibly acting in concert with the inhibition of prototypic neurons that rather promote movement inhibition through an increased activity of BG outputs. With this in mind, movement inhibition induced by the stimulation of the indirect pathway might thus be relying on this dual but synergistic disynaptic mechanism: the classic increased activity of BG output (i.e., through the suppression of prototypic neurons firing) and, in parallel, a suppression of go-related striatal activity (i.e., through the increased firing of arkypallidal neurons). Altogether, the present findings highlight new concepts on the motor function of the indirect pathway. Whether this disynaptic circuit mechanism is also used for BG non-motor function is not known but it is tempting to speculate that it represents a key mechanism by which D2-SPNs can modulate D1-SPN activity[4].

STN Inputs Cause a Disynaptic Inhibition in Arkypallidal Neurons and Can Be Gated by D2-SPN Inputs

It has been shown in mice that optogenetic activation of STN axon terminals within the GPe increases glutamate release[53] and presents a positive bias toward parvalbumin-expressing GPe neurons[54]. We show here that, similar to D2-SPN inputs, STN inputs differentially impact the activity of prototypic and arkypallidal neurons. Our *ex vivo* data demonstrate that both cell populations receive STN excitation but the excitatory currents are smaller in arkypallidal neurons as compared to prototypic neurons. This differential input organization translates into opposite firing responses when studied *in vivo*: STN opto-excitation induces an increased activity of prototypic neurons and a decreased firing in arkypallidal neurons. This opposition in firing rates is in agreement with previous findings in rats[26]. However, we further elucidate here the cellular mechanisms responsible for this opposition of response. Indeed, STN inputs preferentially excite prototypic neurons that, in turn, inhibit arkypallidal neurons through their powerful axon collaterals. This disynaptic mechanism is also revealed when testing the consequences of STN opto-inhibition. Interestingly, we did not find any clear effect of STN opto-excitation when looking at the motor performance of mice walking on a treadmill. This result might appear surprising at first but is consistent with previous findings supporting that STN opto-stimulation produces hyperkinetic behaviors similar to

(H) Typical examples of the activity of an arkypallidal neuron and a prototypic neuron during ON/OFF epochs of light stimulation.
(I) Population PSTHs (left; bin size, 50 ms) and box-and-whisker plots (right) of firing rate changes of all the recorded prototypic neurons during opto-activation of arkypallidal neurons.
Inset bar plots in (F) and (I) represent the percentage of prototypic neurons excited (E), inhibited (I), and unaffected (U) by the light stimulation. Scale bars represent 50 μm (B) or 10 μm (C and D). Group data represent mean ± SEM; box-and-whisker plots indicate median, first and third quartile, and min and max values. **$p < 0.01$; ns, not significant.
See also Table S1 for more details and statistical information.

Please cite this article in press as: Aristieta et al., A Disynaptic Circuit in the Globus Pallidus Controls Locomotion Inhibition, Current Biology (2020), https://doi.org/10.1016/j.cub.2020.11.019

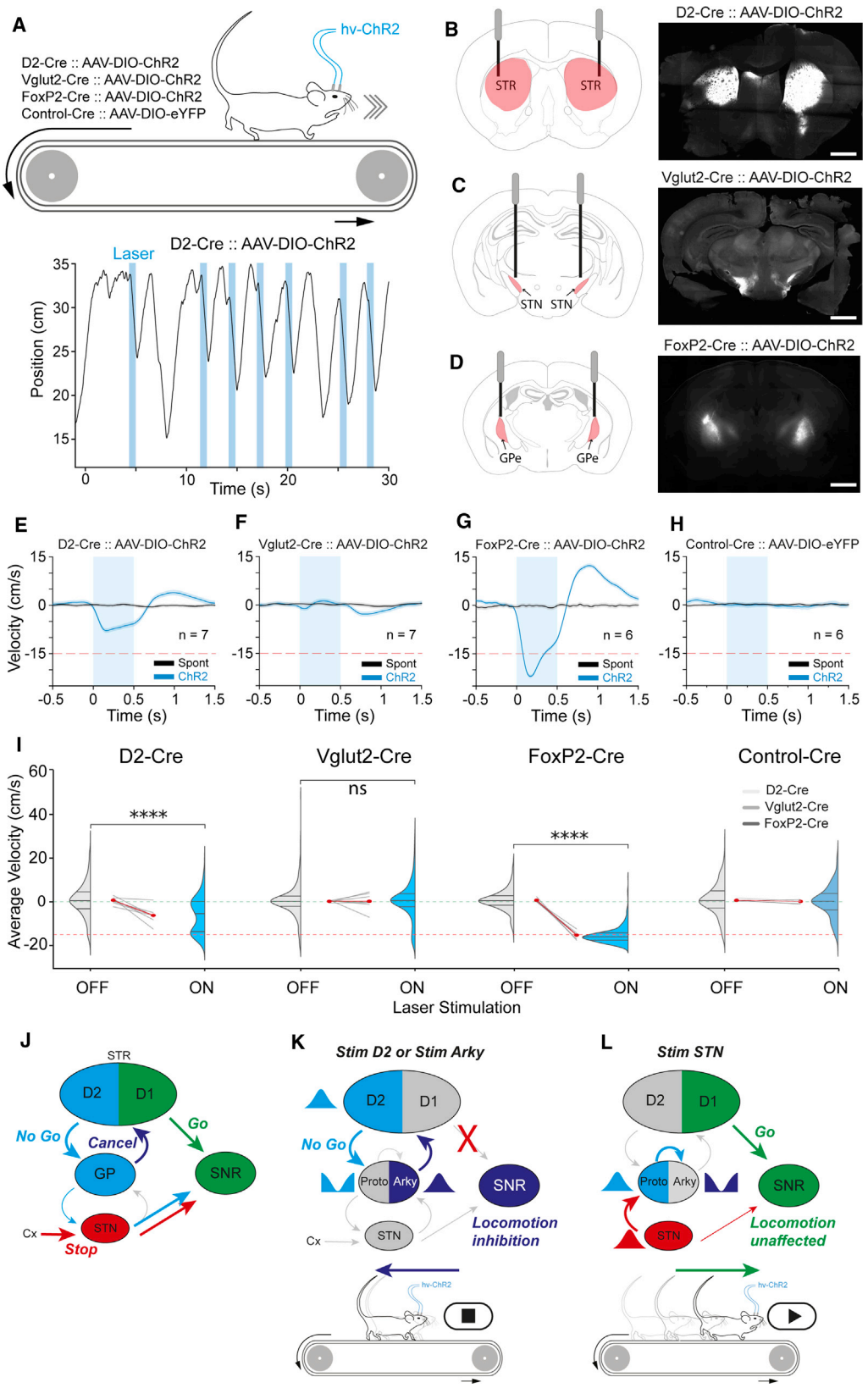

(legend on next page)

Please cite this article in press as: Aristieta et al., A Disynaptic Circuit in the Globus Pallidus Controls Locomotion Inhibition, Current Biology (2020), https://doi.org/10.1016/j.cub.2020.11.019

the ones induced by the direct excitation of GPe neurons[55]. We also believe that this lack of behavioral effect is not caused by the inability of our opto-stimulation to drive further excitation in STN neurons. Indeed, even if the firing of most STN neurons is increased during locomotion[56], the average STN locomotion firing is still lower than the firing rate induced by our light stimulation (i.e., 10 Hz versus 16 Hz, respectively). It is thus likely that STN excitation competes with the STN-induced prototypic increased activity at the level of BG outputs to control movement execution. Moreover, the disynaptic inhibition induced in arkypallidal neurons upon STN opto-excitation will leave striatal go-related signals without arkypallidal inhibitory control (Figure 7L). In addition, our experimental data obtained when co-exciting D2-SPN and STN inputs suggest that D2-SPN neurons are gating the integration of STN inputs in arkypallidal neurons. Indeed, we found that the simultaneous activation of D2-SPNs and STN neurons produces a switch from inhibition to robust excitation in the firing of arkypallidal neurons that is stronger than D2-SPN opto-excitation alone. The end result of this co-activation suggests that STN neurons can now influence the firing of arkypallidal neurons and thus provide a stop signal mediating behavioral inhibition. Importantly, the dysfunction of this gating mechanism could also contribute to the excessive inhibition of movements present in parkinsonism and that has been solely attributed to STN hyperactivity[57].

Prototypic GPe Axon Collaterals Act as a Switch for Arkypallidal Neuronal Activity

Previous work has shown that GPe neurons send axon collaterals to other GPe neurons[27,38,39] and that prototypic neurons project axon collaterals onto arkypallidal neurons[23]. Here, we demonstrate that the axon collaterals from prototypic neurons powerfully control arkypallidal neuronal activity. Interestingly, the collateral connections from arkypallidal to prototypic neurons are not reciprocal or only target a subset of prototypic neurons that were not sampled in our *ex vivo* recordings. Indeed, the population of prototypic neurons has been further divided into subclasses based on the differential expression of molecular markers, projection sites, and differential contribution to motor functions[24,30,33,34,58,59]. Another important aspect for future work is to determine whether specific inputs can directly control the activity of arkypallidal neurons[58,60,61] or whether their activity is always disynaptically controlled by prototypic axon collaterals.

Altogether, our work reveals a novel and unaccounted for disynaptic motif circuit in the GPe that represents an efficient mechanism by which indirect pathway stimulation could inhibit ongoing actions. Our results thus call for a re-evaluation of BG functional organization that should account for the key role played by arkypallidal neurons to control striatal circuits for action selection and cancellation.

STAR★METHODS

Detailed methods are provided in the online version of this paper and include the following:

- KEY RESOURCES TABLE
- RESOURCE AVAILABILITY
  - Lead Contact
  - Materials Availability
  - Data and Code Availability
- EXPERIMENTAL MODEL AND SUBJECT DETAILS
- METHOD DETAILS
  - Stereotaxic injection of viral vectors
  - *In vivo* electrophysiological recording
  - *Ex vivo* electrophysiology recording
  - Drugs
  - Optogenetic stimulation
  - Juxtacellular labeling
  - Histology
  - Behavioral locomotion experiments
- QUANTIFICATION AND STATISTICAL ANALYSIS
  - Data analysis of electrophysiological recordings
  - Data analysis of locomotion
  - Statistics

SUPPLEMENTAL INFORMATION

Supplemental Information can be found online at https://doi.org/10.1016/j.cub.2020.11.019.

ACKNOWLEDGMENTS

This work was supported by grants from the French National Research Agency (ANR-14-CE13-0024-01 and ANR-15-CE37-0006), LABEX BRAIN (ANR-10-LABX-43), and Association France Parkinson (grant OPE-2018-0459). The microscopy was done at the Bordeaux Imaging Center, a service unit of CNRS-INSERM and Bordeaux University, a member of the national infrastructure

Figure 7. Activation of Arkypallidal Neurons Is Sufficient to Induce Locomotion Inhibition

(A) Schematic of the locomotion experiments using a motorized treadmill. D2-Cre, Vglut2-Cre, and FoxP2-Cre mice were injected bilaterally with AAV-DIO-ChR2-eYFP or control AAV-DIO-eYFP in the STR (n = 7 and n = 2, respectively), STN (n = 7 and n = 2, respectively), and GPe (n = 7 and n = 2, respectively). Raw example (bottom) of 30-s locomotion bouts in D2-Cre::AAV-ChR2 mice receiving blue light stimulation (500 ms long) at random timing.

(B–D) Brain schematics with optic fiber positions in the target areas and corresponding epifluorescent images illustrating the histological verification of the ChR2-eYFP virus expression in D2-Cre (B), Vglut2-Cre (C), and FoxP2-Cre mice (D) (the scale bars represent 1 mm).

(E–H) Average velocity induced by the light stimulation (blue) or during spontaneous locomotion (black) in D2-Cre::AAV-ChR2 (E), Vglut2-Cre::AAV-ChR2 (F), FoxP2-Cre::AAV-ChR2 (G), and all the various control mouse experiments (Control-Cre::AAV-eYFP; H).

(I) Velocity population graphs showing the velocity distributions during laser ON/OFF in the different animals. The gray lines represent individual animals and the red lines represent the mean between animals. The dotted red line shows the velocity of the treadmill (15 cm/s).

(J) Classic BG schematic illustrating the multiple pathways controlling locomotion.

(K) Activation of the indirect pathway (D2) suppresses activity in prototypic (Proto) neurons, which turns ON arkypallidal neurons (Arky) and inhibits locomotion.

(L) Stimulation of the hyperdirect pathway (STN) produces the opposite effect on prototypic and arkypallidal neuronal activity but fails to inhibit movement.

Group data represent mean ± SEM; distribution plots indicate median, first and third quartile, and min and max values. ****$p < 0.0001$; ns, not significant. Cx, cortex.

See also Table S1 for more details and statistical information.

France BioImaging supported by the French National Research Agency (ANR-10-INBS-04). We also thank the PIV-EXPE of the University of Bordeaux and the Ani*Motion* collaborative facility (INCIA). The University of Bordeaux and CNRS provided infrastructural support. We are grateful to E. Doudnikoff, Monika Fernández-Monreal, A. Fayoux, R. Kinet, T. Nguyen, and H. Orignac for technical assistance as well as Drs. R. Schmidt, A. Leblois, G. Silberberg, F. Georges, M. Deffains, and R. Bidgood for insightful scientific discussions and comments on the manuscript.

AUTHOR CONTRIBUTIONS

B.d.l.C. and N.P.M. performed the proof-of-concept experiments. J.B. and N.P.M. conceptualized the project. A.A., B.d.l.C., L.G., S.G., and N.P.M. performed *in vivo* electrophysiology recordings. M.B. and J.B. performed slice electrophysiology recordings. A.A., S.F., M.B., and N.P.M. performed histology. A.A., S.A.L., G.B., and N.P.M. performed behavioral experiments. A.A., M.B., J.B., S.A.L., G.C., and N.P.M. performed the analysis. J.B. and N.P.M. designed the experiments and supervised the project. A.A., M.B., J.B., and N.P.M. wrote the manuscript.

DECLARATION OF INTERESTS

The authors declare no competing interests.

Received: September 24, 2020
Revised: November 5, 2020
Accepted: November 5, 2020
Published: December 10, 2020

REFERENCES

1. Grillner, S., Robertson, B., and Stephenson-Jones, M. (2013). The evolutionary origin of the vertebrate basal ganglia and its role in action selection. J. Physiol. *591*, 5425–5431.
2. Cox, J., and Witten, I.B. (2019). Striatal circuits for reward learning and decision-making. Nat. Rev. Neurosci. *20*, 482–494.
3. Hwang, E.J., Link, T.D., Hu, Y.Y., Lu, S., Wang, E.H.J., Lilascharoen, V., Aronson, S., O'Neil, K., Lim, B.K., and Komiyama, T. (2019). Corticostriatal flow of action selection bias. Neuron *104*, 1126–1140.e6.
4. Matamales, M., McGovern, A.E., Mi, J.D., Mazzone, S.B., Balleine, B.W., and Bertran-Gonzalez, J. (2020). Local D2- to D1-neuron transmodulation updates goal-directed learning in the striatum. Science *367*, 549–555.
5. Roseberry, T.K., Lee, A.M., Lalive, A.L., Wilbrecht, L., Bonci, A., and Kreitzer, A.C. (2016). Cell-type-specific control of brainstem locomotor circuits by basal ganglia. Cell *164*, 526–537.
6. Rueda-Orozco, P.E., and Robbe, D. (2015). The striatum multiplexes contextual and kinematic information to constrain motor habits execution. Nat. Neurosci. *18*, 453–460.
7. Tecuapetla, F., Jin, X., Lima, S.Q., and Costa, R.M. (2016). Complementary contributions of striatal projection pathways to action initiation and execution. Cell *166*, 703–715.
8. Yttri, E.A., and Dudman, J.T. (2016). Opponent and bidirectional control of movement velocity in the basal ganglia. Nature *533*, 402–406.
9. Alexander, G.E., and Crutcher, M.D. (1990). Functional architecture of basal ganglia circuits: neural substrates of parallel processing. Trends Neurosci. *13*, 266–271.
10. Albin, R.L., Young, A.B., and Penney, J.B. (1989). The functional anatomy of basal ganglia disorders. Trends Neurosci. *12*, 366–375.
11. Hikosaka, O. (2007). GABAergic output of the basal ganglia. Prog. Brain Res. *160*, 209–226.
12. Cebrián, C., Parent, A., and Prensa, L. (2005). Patterns of axonal branching of neurons of the substantia nigra pars reticulata and pars lateralis in the rat. J. Comp. Neurol. *492*, 349–369.
13. Morrissette, A.E., Chen, P.H., Bhamani, C., Borden, P.Y., Waiblinger, C., Stanley, G.B., and Jaeger, D. (2019). Unilateral optogenetic inhibition and excitation of basal ganglia output affect directional lick choices and movement initiation in mice. Neuroscience *423*, 55–65.
14. Rossi, M.A., Li, H.E., Lu, D., Kim, I.H., Bartholomew, R.A., Gaidis, E., Barter, J.W., Kim, N., Cai, M.T., Soderling, S.H., and Yin, H.H. (2016). A GABAergic nigrotectal pathway for coordination of drinking behavior. Nat. Neurosci. *19*, 742–748.
15. Kravitz, A.V., Freeze, B.S., Parker, P.R.L., Kay, K., Thwin, M.T., Deisseroth, K., and Kreitzer, A.C. (2010). Regulation of parkinsonian motor behaviours by optogenetic control of basal ganglia circuitry. Nature *466*, 622–626.
16. Schmidt, R., Leventhal, D.K., Mallet, N., Chen, F., and Berke, J.D. (2013). Canceling actions involves a race between basal ganglia pathways. Nat. Neurosci. *16*, 1118–1124.
17. Jin, X., and Costa, R.M. (2010). Start/stop signals emerge in nigrostriatal circuits during sequence learning. Nature *466*, 457–462.
18. Chevalier, G., and Deniau, J.M. (1990). Disinhibition as a basic process in the expression of striatal functions. Trends Neurosci. *13*, 277–280.
19. Pasquereau, B., and Turner, R.S. (2017). A selective role for ventromedial subthalamic nucleus in inhibitory control. eLife *6*, 1–27.
20. Cazorla, M., Kang, U.J., and Kellendonk, C. (2015). Balancing the basal ganglia circuitry: a possible new role for dopamine D2 receptors in health and disease. Mov. Disord. *30*, 895–903.
21. Gittis, A.H., Berke, J.D., Bevan, M.D., Chan, C.S., Mallet, N., Morrow, M.M., and Schmidt, R. (2014). New roles for the external globus pallidus in basal ganglia circuits and behavior. J. Neurosci. *34*, 15178–15183.
22. Kita, H. (2007). Globus pallidus external segment. Prog. Brain Res. *160*, 111–133.
23. Mallet, N., Micklem, B.R., Henny, P., Brown, M.T., Williams, C., Bolam, J.P., Nakamura, K.C., and Magill, P.J. (2012). Dichotomous organization of the external globus pallidus. Neuron *74*, 1075–1086.
24. Mastro, K.J., Zitelli, K.T., Willard, A.M., Leblanc, K.H., Kravitz, A.V., and Gittis, A.H. (2017). Cell-specific pallidal intervention induces long-lasting motor recovery in dopamine-depleted mice. Nat. Neurosci. *20*, 815–823.
25. Mallet, N., Schmidt, R., Leventhal, D., Chen, F., Amer, N., Boraud, T., and Berke, J.D. (2016). Arkypallidal cells send a stop signal to striatum. Neuron *89*, 308–316.
26. Crompe, B., Aristieta, A., Leblois, A., Elsherbiny, S., Boraud, T., and Mallet, N.P. (2020). The globus pallidus orchestrates abnormal network dynamics in a model of parkinsonism. Nat. Commun. *11*, 1570.
27. Sato, F., Lavallée, P., Lévesque, M., and Parent, A. (2000). Single-axon tracing study of neurons of the external segment of the globus pallidus in primate. J. Comp. Neurol. *417*, 17–31.
28. Fujiyama, F., Nakano, T., Matsuda, W., Furuta, T., Udagawa, J., and Kaneko, T. (2016). A single-neuron tracing study of arkypallidal and prototypic neurons in healthy rats. Brain Struct. Funct. *221*, 4733–4740.
29. Bevan, M.D., Booth, P.A.C., Eaton, S.A., and Bolam, J.P. (1998). Selective innervation of neostriatal interneurons by a subclass of neuron in the globus pallidus of the rat. J. Neurosci. *18*, 9438–9452.
30. Mastro, K.J., Bouchard, R.S., Holt, H.A., and Gittis, A.H. (2014). Transgenic mouse lines subdivide external segment of the globus pallidus (GPe) neurons and reveal distinct GPe output pathways. J. Neurosci *34*, 2087–2099.
31. Glajch, K.E., Kelver, D.A., Hegeman, D.J., Cui, Q., Xenias, H.S., Augustine, E.C., Hernández, V.M., Verma, N., Huang, T.Y., Luo, M., et al. (2016). Npas1+ pallidal neurons target striatal projection neurons. J. Neurosci. *36*, 5472–5488.
32. Smith, Y., Bevan, M.D., Shink, E., and Bolam, J.P. (1998). Microcircuitry of the direct and indirect pathways of the basal ganglia. Neuroscience *86*, 353–387.
33. Dodson, P.D., Larvin, J.T., Duffell, J.M., Garas, F.N., Doig, N.M., Kessaris, N., Duguid, I.C., Bogacz, R., Butt, S.J.B., and Magill, P.J. (2015). Distinct developmental origins manifest in the specialized encoding of movement by adult neurons of the external globus pallidus. Neuron *86*, 501–513.

34. Abdi, A., Mallet, N., Mohamed, F.Y., Sharott, A., Dodson, P.D., Nakamura, K.C., Suri, S., Avery, S.V., Larvin, J.T., Garas, F.N., et al. (2015). Prototypic and arkypallidal neurons in the dopamine-intact external globus pallidus. J. Neurosci. *35*, 6667–6688.

35. Abrahao, K.P., and Lovinger, D.M. (2018). Classification of GABAergic neuron subtypes from the globus pallidus using wild-type and transgenic mice. J. Physiol. *596*, 4219–4235.

36. Hernández, V.M., Hegeman, D.J., Cui, Q., Kelver, D.A., Fiske, M.P., Glajch, K.E., Pitt, J.E., Huang, T.Y., Justice, N.J., and Chan, C.S. (2015). Parvalbumin+ neurons and Npas1+ neurons are distinct neuron classes in the mouse external globus pallidus. J. Neurosci. *35*, 11830–11847.

37. Cazorla, M., de Carvalho, F.D., Chohan, M.O., Shegda, M., Chuhma, N., Rayport, S., Ahmari, S.E., Moore, H., and Kellendonk, C. (2014). Dopamine D2 receptors regulate the anatomical and functional balance of basal ganglia circuitry. Neuron *81*, 153–164.

38. Kita, H., and Kitai, S.T. (1994). The morphology of globus pallidus projection neurons in the rat: an intracellular staining study. Brain Res. *636*, 308–319.

39. Sadek, A.R., Magill, P.J., and Bolam, J.P. (2007). A single-cell analysis of intrinsic connectivity in the rat globus pallidus. J. Neurosci. *27*, 6352–6362.

40. Kovaleski, R.F., Callahan, J.W., Chazalon, M., Wokosin, D.L., Baufreton, J., and Bevan, M.D. (2020). Dysregulation of external globus pallidus-subthalamic nucleus network dynamics in parkinsonian mice during cortical slow-wave activity and activation. J. Physiol. *598*, 1897–1927.

41. Kita, H., and Kitai, S.T. (1987). Efferent projections of the subthalamic nucleus in the rat: light and electron microscopic analysis with the PHA-L method. J. Comp. Neurol. *260*, 435–452.

42. Smith, Y., Hazrati, L.N., and Parent, A. (1990). Efferent projections of the subthalamic nucleus in the squirrel monkey as studied by the PHA-L anterograde tracing method. J. Comp. Neurol. *294*, 306–323.

43. Miguelez, C., Morin, S., Martinez, A., Goillandeau, M., Bezard, E., Bioulac, B., and Baufreton, J. (2012). Altered pallido-pallidal synaptic transmission leads to aberrant firing of globus pallidus neurons in a rat model of Parkinson's disease. J. Physiol. *590*, 5861–5875.

44. Bugaysen, J., Bar-Gad, I., and Korngreen, A. (2013). Continuous modulation of action potential firing by a unitary GABAergic connection in the globus pallidus *in vitro*. J. Neurosci. *33*, 12805–12809.

45. Ketzef, M., and Silberberg, G. (2020). Differential synaptic input to external globus pallidus neuronal subpopulations *in vivo*. Neuron. https://doi.org/10.1016/j.neuron.2020.11.006.

46. Cui, G., Jun, S.B., Jin, X., Pham, M.D., Vogel, S.S., Lovinger, D.M., and Costa, R.M. (2013). Concurrent activation of striatal direct and indirect pathways during action initiation. Nature *494*, 238–242.

47. Durieux, P.F., Bearzatto, B., Guiducci, S., Buch, T., Waisman, A., Zoli, M., Schiffmann, S.N., and de Kerchove d'Exaerde, A. (2009). D2R striatopallidal neurons inhibit both locomotor and drug reward processes. Nat. Neurosci. *12*, 393–395.

48. Oldenburg, I.A., and Sabatini, B.L. (2015). Antagonistic but not symmetric regulation of primary motor cortex by basal ganglia direct and indirect pathways. Neuron *86*, 1174–1181.

49. Panigrahi, B., Martin, K.A., Li, Y., Graves, A.R., Vollmer, A., Olson, L., Mensh, B.D., Karpova, A.Y., and Dudman, J.T. (2015). Dopamine is required for the neural representation and control of movement vigor. Cell *162*, 1418–1430.

50. Sheng, M.J., Lu, D., Shen, Z.M., and Poo, M.M. (2019). Emergence of stable striatal D1R and D2R neuronal ensembles with distinct firing sequence during motor learning. Proc. Natl. Acad. Sci. USA *116*, 11038–11047.

51. Chuhma, N., Tanaka, K.F., Hen, R., and Rayport, S. (2011). Functional connectome of the striatal medium spiny neuron. J. Neurosci. *31*, 1183–1192.

52. Kita, H., and Kitai, S.T. (1991). Intracellular study of rat globus pallidus neurons: membrane properties and responses to neostriatal, subthalamic and nigral stimulation. Brain Res. *564*, 296–305.

53. Viereckel, T., Konradsson-Geuken, Å., and Wallén-Mackenzie, Å. (2018). Validated multi-step approach for *in vivo* recording and analysis of optogenetically evoked glutamate in the mouse globus pallidus. J. Neurochem. *145*, 125–138.

54. Pamukcu, A., Cui, Q., Xenias, H.S., Berceau, B.L., Augustine, E.C., Fan, I., Chalasani, S., Hantman, A.W., Lerner, T.N., Boca, S.M., and Chan, C.S. (2020). Parvalbumin+ and Npas1+ pallidal neurons have distinct circuit topology and function. J. Neurosci. *40*, 7855–7876.

55. Tian, J., Yan, Y., Xi, W., Zhou, R., Lou, H., Duan, S., Chen, J.F., and Zhang, B. (2018). Optogenetic stimulation of GABAergic neurons in the globus pallidus produces hyperkinesia. Front. Behav. Neurosci. *12*, 185.

56. Shi, L.H., Luo, F., Woodward, D.J., and Chang, J.Y. (2004). Neural responses in multiple basal ganglia regions during spontaneous and treadmill locomotion tasks in rats. Exp. Brain Res. *157*, 303–314.

57. Bergman, H., Wichmann, T., and DeLong, M.R. (1990). Reversal of experimental parkinsonism by lesions of the subthalamic nucleus. Science *249*, 1436–1438.

58. Abecassis, Z.A., Berceau, B.L., Win, P.H., García, D., Xenias, H.S., Cui, Q., Pamukcu, A., Cherian, S., Hernández, V.M., Chon, U., et al. (2020). Npas1^{+}-Nkx2.1^{+} neurons are an integral part of the cortico-pallido-cortical loop. J. Neurosci. *40*, 743–768.

59. Saunders, A., Oldenburg, I.A., Berezovskii, V.K., Johnson, C.A., Kingery, N.D., Elliott, H.L., Xie, T., Gerfen, C.R., and Sabatini, B.L. (2015). A direct GABAergic output from the basal ganglia to frontal cortex. Nature *521*, 85–89.

60. Karube, F., Takahashi, S., Kobayashi, K., and Fujiyama, F. (2019). Motor cortex can directly drive the globus pallidus neurons in a projection neuron type-dependent manner in the rat. eLife *8*, 1–79.

61. Hunt, A.J., Jr., Dasgupta, R., Rajamanickam, S., Jiang, Z., Beierlein, M., Chan, C.S., and Justice, N.J. (2018). Paraventricular hypothalamic and amygdalar CRF neurons synapse in the external globus pallidus. Brain Struct. Funct. *223*, 2685–2698.

62. Jackman, S.L., Beneduce, B.M., Drew, I.R., and Regehr, W.G. (2014). Achieving high-frequency optical control of synaptic transmission. J. Neurosci. *34*, 7704–7714.

63. Pinault, D. (1996). A novel single-cell staining procedure performed *in vivo* under electrophysiological control: morpho-functional features of juxtacellularly labeled thalamic cells and other central neurons with biocytin or neurobiotin. J. Neurosci. Methods *65*, 113–136.

64. Schindelin, J., Arganda-Carreras, I., Frise, E., Kaynig, V., Longair, M., Pietzsch, T., Preibisch, S., Rueden, C., Saalfeld, S., Schmid, B., et al. (2012). Fiji: an open-source platform for biological-image analysis. Nat. Methods *9*, 676–682.

65. Deister, C.A., Dodla, R., Barraza, D., Kita, H., and Wilson, C.J. (2013). Firing rate and pattern heterogeneity in the globus pallidus arise from a single neuronal population. J. Neurophysiol. *109*, 497–506.

66. Mathis, A., Mamidanna, P., Cury, K.M., Abe, T., Murthy, V.N., Mathis, M.W., and Bethge, M. (2018). DeepLabCut: markerless pose estimation of user-defined body parts with deep learning. Nat. Neurosci. *21*, 1281–1289.

Please cite this article in press as: Aristieta et al., A Disynaptic Circuit in the Globus Pallidus Controls Locomotion Inhibition, Current Biology (2020), https://doi.org/10.1016/j.cub.2020.11.019

STAR★METHODS

KEY RESOURCES TABLE

REAGENT or RESOURCE	SOURCE	IDENTIFIER
Antibodies		
Chicken anti-GFP antibody	Aves Labs	Cat#GFP-1020; RRID:AB_10000240
Rabbit anti-GFP antibody	Life Technologies	CAT#A11122; RRID:AB_221569
Mouse anti-GFP antibody	Roche	Cat#11814460001; RRID:AB_390913
Rat anti-RFP antibody	Chromotek	CAT#5f8; **RRID:**AB_2336064
Rabbit anti-RFP antibody	Life Technologies	Cat# R10367; RRID:AB_10563941
Rabbit anti-Nkx2.1 (TTF-1) antibody	Santa Cruz Biotechnology	Cat#sc-13040; RRID:AB_793532
Goat anti-FoxP2 antibody	Santa Cruz Biotechnology	Cat#sc-21069; RRID:AB_2107124
Rabbit anti-Preproenkephalin	LifeSpan Biosciences	Cat# LS-C23084-50; RRID:AB_902714
Alexa Fluor 488 AffiniPure Donkey Anti-Chicken	Jackson ImmunoResearch Labs	Cat# 703-545-155; RRID:AB_2340375
CY5-conjugated Donkey Anti-Rabbit	Jackson ImmunoResearch Labs	Cat# 711-175-152; RRID:AB_2340607
Brilliant Violet 421-conjugated Donkey Anti-Goat	Jackson ImmunoResearch Labs	Cat# 705-675-147; RRID:AB_2651102
Alexa Fluor 488 Donkey anti-Rabbit	Life Technologies	CAT#A21206; RRID:AB_2535792
Alexa Fluor 488 Donkey anti-Mouse	Life Technologies	Cat#A 21202; RRID:AB_141607
Alexa Fluor 568 Donkey anti-Rabbit	Life Technologies	Cat#A10042; RRID: AB_2534017
Alexa Fluor 594 Donkey anti-Rat	Life Technologies	CAT#A21209; RRID: AB_2535795
Alexa Fluor 647 Donkey anti-Goat	Life Technologies	Cat#A21447; RRID: AB_2535864
Bacterial and Virus Strains		
AAV5-EF1α-DIO-ChR2(H134R)-EYFP	University of North Carolina at Chapel Hill Vector Core (UNC)	Lot#AV4313x $7x10^{12}$ virus mol/ml
AAV5-EF1α-DIO-ChR2(H134R)-mCherry	University of North Carolina at Chapel Hill Vector Core (UNC)	Lot#AV4314I $5.2x10^{12}$ virus mol/ml
AAV5-EF1α-DIO-EYFP	University of North Carolina at Chapel Hill Vector Core (UNC)	Lot#AV4310J $6.5x10^{12}$ virus mol/ml
AAV5-CAG-Flex-ArchT-tdTomato	University of North Carolina at Chapel Hill Vector Core (UNC)	Lot#AV4567bc $6x10^{12}$ virus mol/ml

(*Continued on next page*)

Please cite this article in press as: Aristieta et al., A Disynaptic Circuit in the Globus Pallidus Controls Locomotion Inhibition, Current Biology (2020), https://doi.org/10.1016/j.cub.2020.11.019

CellPress
OPEN ACCESS

Continued

REAGENT or RESOURCE	SOURCE	IDENTIFIER
Chemicals, Peptides, and Recombinant Proteins		
Isoflurane	Piramal Healthcare UK Limited	Iso-vet®; CAS: 26675-46-7
Lidocaine	AstraZeneca	Xylocaine®; CAS: 137-58-6
Ophthalmic ointment	Bauch & Lomb Swiss	liposic®
D-(+)-Glucose	Sigma-Aldrich	CAT#G8270; CAS: 50-99-7
Buprenorphine	Axience	Buprecare®; CAS: 52485-79-7
Urethane	Sigma-Aldrich	CAT#U2500; CAS: 51-79-6
Neurobiotin tracer	Vector laboratories	CAT#SP-1120
Biocytin	Sigma-Aldrich	CAT#B4261
Normal Donkey Serum	EuroBio	CAT#CAEANE000U, RRID:AB_2753145
Pentobarbital sodium	Axience	Exagon®; CAS: 57-33-0
Formaldehyde	VWR	CAT#20909.330; CAS: 50-00-0
Vectashield medium	Vector laboratories	CAT#H-1000
Triton X-100	Sigma-Aldrich	CAT#T9284
Streptavidine-CY3 Zymax	Life Technologies	CAT#438315
Streptavidine 488	Life Technologies	CAT#S11223
Streptavidine 557	R&D systems	CAT#NL999
Streptavidine 568	Life Technologies	CAT#S11226
DNQX disodium salt	Bio-Techne	CAT#2312
D-APV	Bio-Techne	CAT#0106
SR 95531 hydrochloride	Bio-Techne	CAT#1262
QX-314 hydrobromide	Bio-Techne	CAT#1014
Experimental Models: Organisms/Strains		
Mouse: *Drd2-cre*: B6.FVB(Cg)-Tg(Drd2-cre) ER44Gsat/Mmucd	MMRRC	RRID:MMRRC_032108-UCD:
Mouse: *Vglut2-ires-cre*: Slc17a6$^{tm2(cre)Lowl}$/J	Jackson Laboratory	RRID:IMSR_JAX:016963
Mouse: *Nkx2.1-Cre*: C57BL/6J-Tg(Nkx2-1-cre)2Sand/J	Jackson Laboratory	RRID:IMSR_JAX:008661
Mouse: *FoxP2-cre*: B6.Cg-Foxp2 < tm1.1(cre/GFP)Rpa > /J	Jackson Laboratory	RRID:IMSR_JAX:030541
Mouse: *Ai32*: B6.Cg-*Gt(ROSA)26Sor*$^{tm32(CAG-COP4*H134R/EYFP)Hze}$/J	Jackson Laboratory	RRID:IMSR_JAX: 024109
Mouse: *Drd2-cre::Ai32*	University of Bordeaux Animal facility (CRYME)	N/A
Mouse: *Drd2-cre::Vglut2-ires-cre*	University of Bordeaux Animal facility (CRYME)	N/A
Software and Algorithms		
Spike2 Software	Cambridge Electronic Design	RRID: SCR_000903
MATLAB®	MathWorks	RRID: SCR_001622
Graphpad Prism 8 (version 8.4.3)	Graphpad software Inc	RRID: SCR_002798
Fiji	https://imagej.net/Fiji	RRID: SCR_002285
Adobe Illustrator	Adobe Systems	RRID: SCR_014198

(*Continued on next page*)

Please cite this article in press as: Aristieta et al., A Disynaptic Circuit in the Globus Pallidus Controls Locomotion Inhibition, Current Biology (2020), https://doi.org/10.1016/j.cub.2020.11.019

Continued

REAGENT or RESOURCE	SOURCE	IDENTIFIER
Adobe Photoshop	Adobe Systems	RRID:SCR_014199
Python Programming Language		RRID:SCR_008394
pClamp 10 (version 10.3 & 10.6)	Molecular Devices	RRID:SCR_011323
Origin	MicroCal Origin	RRID:SCR_002815

RESOURCE AVAILABILITY

Lead Contact

Further information and request for resources should be directed to and will be fulfilled by the Lead Contact, Nicolas Mallet (nicolas.mallet@u-bordeaux.fr).

Materials Availability

This study did not generate new unique reagents.

Data and Code Availability

The codes for the analysis used in this study are available from the corresponding authors upon request. The raw data from the current study were not deposited into a public repository due to the large size of the datasets, but are available from the corresponding authors upon reasonable request. The primary dataset underlying the figures are publicly available via figshare following this link: https://figshare.com/s/eefda44192b5a9846b97.

EXPERIMENTAL MODEL AND SUBJECT DETAILS

All Experimental procedures were performed on both male and female adult (> 6 weeks) mice with C57BL/6J genetic backgrounds in accordance with the European legislation for the protection of animals used for scientific purposes (directive 2010/63/EU). D2-SPNs were specifically targeted using D2-Cre mouse line (GENSAT, catalog no. 032108-UCD), STN neurons were targeted using Vglut2-Cre mouse line (The Jackson Laboratory, stock no. 016963), prototypic GPe neurons were targeted using Nkx2.1-Cre mouse line (The Jackson Laboratory, stock no. 008661), and arkypallidal GPe neurons were targeted using the FoxP2-Cre mouse line (The Jackson Laboratory, stock no. 030541). To enable targeting of both D2-SPNs and STN neurons in the same animals, we generated a D2-Cre::Vglut2-Cre mouse line by breeding hemizygous Vglut2-Cre driver mice with homozygous D2-Cre mice. To promote ChR2 expression in all D2-SPNs we generated a D2-Cre::Ai32 mice by breeding D2-cre driver mice with homozygous Ai32 mice (The Jackson Laboratory, stock no. 024109). This project was approved by the French ministry of higher education and research and the ethical committee of CNRS, Aquitaine Region (accreditation numbers #6231 and #25001). Mice were housed collectively (at least by 2 per cage) under artificial conditions of light (light/dark cycle, light on at 7:00 a.m.), temperature (24°C), and humidity (45%) with food and water available *ad libitum*. A total number of 151 mice were used for this study of which 12 mice were excluded due to failed or missed virus injection associated both with low transduction rate of targeted area.

METHOD DETAILS

Stereotaxic injection of viral vectors

All the virus used for our optogenetic manipulations were adeno-associated virus directly purchased from a vector core (UNC vector core) and micro-injected under stereotaxic condition in D2-Cre, Vglut2-Cre, double D2-Cre::Vglut2-Cre, Nkx2.1-Cre, and FoxP2-Cre mice using glass capillary (tip diameter 35 μm; 1-5 μL Hirschmann® microcapillary pipette, CAT#Z611239, Sigma-Aldrich) connected to a Picospritzer® pressure system (Parker Hannifin). Briefly, mice were anesthetized with isoflurane (induction/maintenance: 3-5/1.5%; Iso-vet®, Piramal healthcare), fixed on a stereotaxic frame (Unimécanique, M2e) and placed on heating blanket. An ophthalmic ointment (Liposic®, Bauch & Lomb Swiss) was used all along the surgery to prevent dehydration. Photo-stimulation of D2-SPNs or STN neurons were performed using an AAV5-EF1α-DIO-ChR2(H134R)-eYFP viral vector ($4x10^{12}$ viral particles/mL) injected in D2-Cre mice (n = 80, 2 points of injections in dorsolateral striatum at coordinates AP: 0.8 mm and 0.3 mm anterior to bregma, ML: 1.75 mm and 2.2 mm, DV: 2.6 mm, volume: 400 nL per site) or Vglut2-Cre mice (n = 61, injection in STN at coordinates AP: 1.8 mm posterior to bregma, ML: 1.5 mm, and DV: 4.5 mm, volume: 150 nL per site). Photo-inhibition of STN neurons were performed using an AAV5-CAG-Flex-ArchT-tdTomato ($6x10^{12}$ viral particles/mL), injected in the STN of Vglut2-Cre mice (n = 8, same coordinates as above). Combined injections of these viruses were used for dual photo-excitation of both D2-SPNs and STN inputs (n = 12 D2-Cre::Vglut2-Cre mice) or photo-excitation and photo-inhibition of D2-SPNs and STN inputs, respectively

Please cite this article in press as: Aristieta et al., A Disynaptic Circuit in the Globus Pallidus Controls Locomotion Inhibition, Current Biology (2020), https://doi.org/10.1016/j.cub.2020.11.019

(n = 10 D2-Cre::Vglut2-Cre mice). Photo-excitation of prototypic or arkypallidal neurons were performed using an AAV5-EF1α-DIO-ChR2(H134R)-mCherry ($5.2x10^{12}$ viral particles/mL) injected in the GPe (coordinates AP: 0.35 mm posterior to bregma, ML: 2.0 mm, DV: 3.6 mm, volume: 120-200 nL per site) of Nkx2.1-Cre (n = 7) or FoxP2-Cre (n = 9) animals, respectively.

For the behavioral locomotion experiments, opto-excitation experiments were performed in animals (D2-Cre, n = 7; Vglut2-Cre, n = 7; FoxP2-Cre, n = 6) that were injected bilaterally into the region of interest (i.e., striatum, STN, or GPe) using the same virus as the one used for electrophysiological experiments: an AAV5-EF1α-DIO-ChR2(H134R)-eYFP (for D2-Cre and Vglut2-Cre mice) or an AAV5-EF1α-DIO-ChR2(H134R)-mCherry (for FoxP2-cre) at similar coordinates and volume as aforementioned. To control for a light effect on locomotion, we additionally performed opto-control experiments in animals (D2-Cre, n = 2; Vglut2-Cre, n = 2; FoxP2-Cre, n = 2) injected bilaterally (in similar target regions) with the control virus AAV5-EF1α-DIO-eYFP ($6.5x10^{12}$ viral particles/mL). Then, two ceramic optic fibers (CFX128, ThorLab) were implanted bilaterally within the dorsolateral striatum (AP: 1.2 mm anterior to bregma, ML: 1.9 mm, DV: −2.0 mm) the STN (AP: −2.0 mm posterior to bregma, ML: 1.5 mm, DV: −3.9 mm,), and the GPe (AP: 0.35 mm posterior to bregma, ML: 1.9 mm, DV: −2.9 mm).

In vivo electrophysiological recording

Electrophysiological recordings and optogenetic manipulations were realized at least 3 weeks after viral transduction under urethane anesthesia. Anaesthesia was first induced with isoflurane (3%–5%; Iso-vet®, Piramal healthcare), and maintained with urethane (i.p., 1.3g/Kg.; CAT#U2500, Sigma-Aldrich). The animals were then secured in a stereotaxic frame (Unimécanique, M2e) and placed on heating blanket. After subcutaneous injection of xylocain, skull was exposed and craniotomies were performed to enable electrophysiological recordings and optogenetic stimulation of the region of interest (same stereotaxic coordinates as above). In each mouse, an electrocorticogram (ECoG) of the sensorimotor cortex was realized (AP: 2.2 mm rostral to bregma, ML: 2.1 mm) with a 1 mm screw juxtaposed to the dura mater. All along the recording session, saline solution was used to prevent dehydration and anesthesia level was frequently controlled by examination of EcoG and by testing the response of gentled sensory stimuli (tail pinch).

In vivo extracellular recordings were performed using glass electrodes (1-3μm tip end, 12-20MΩ, GC150F, WPI) filled with a chloride solution 0.5 M containing neurobiotin tracer (1%–2%, w/v; CAT#SP-1120, Vector laboratories) to perform juxtacellular labeling. Optogenetic manipulation of the recorded neurons were performed using optical fibers placed in the striatum and/or the STN and an opto-electrode, homemade by gluing an optical fiber (multimode Fiber, 0.22NA, core diameter: 105μm, Thorlabs) 1mm from the tip of the glass electrodes. This method allows to combin extracellular recording, juxtacellular labeling, and optogenetic manipulation. Once opto-electrode was implanted in the recording structure, the signal was amplified by 10-fold in axoClamp 2B (in bridge mode; Molecular Devices). Then, recording signal was amplified 1000 fold and filtered with differential AC amplifier (spike unit: 0.3-10 kHz, local field potential: 0.1Hz-10 kHz; model 1700, A-M Systems). For ECoG recording, the signal was amplified 1000 fold and filtered with the same differential AC amplifier (0.1Hz-5 kHz). Finally, the recorded signals were digitalized at 20 kHz, by using the Power1401-3 connected to a computer equipped with Spike2 software (version 8, Cambridge Electronic Design).

To identify the location of the recorded unit we performed juxtacellular labeling as previously described[23]. Then histological validation of the labeled neurons and the recording track of the electrode confirmed the recording locations. This approach has been used for all our experiments.

Ex vivo electrophysiology recording

Mice with an age range of 56-105 postnatal day were sedated with isoflurane, deeply anesthetized with an i.p. injection of ketamine/xylazine (75/10 mg/Kg) cocktail and then perfused transcardially with cold (0-4°C) modified artificial cerebrospinal fluid (ACSF), continuously oxygenated with carbogen (95% O_2 - 5% CO_2) and containing the following (in mM): 230 sucrose, 26 $NaHCO_3$, 2.5 KCl, 1.25 NaH_2PO_4, 0.5 $CaCl_2$, 10 $MgSO_4$ and 10 glucose (pH∼7,35). The Brain was rapidly removed, glued to the stage of a vibratome (VT1200S; Leica Microsystems, Germany), immersed in the ice-cold ACSF and sectioned into 300 μm thick parasagittal or coronal slices. Slices containing the STR, GPe and STN were transferred for 1 hour to a standard ACSF solution, warmed (35°C) and equilibrated with carbogen and containing (in mM unless otherwise stated): 126 NaCl, 26 $NaHCO_3$, 2.5 KCl, 1.25 NaH_2PO_4, 2 $CaCl_2$, 2 $MgSO_4$, 10 glucose, 1 sodium pyruvate and 4.9 μM L-gluthathione reduced. Single slices were then transferred to a recording chamber, perfused continuously with equilibrated ACSF (without sodium pyruvate and L-gluthathione) heated at 32-34°C, and visualized using infrared gradient contrast video microscopy (Ni-e workstation, Nikon) and a 60X water-immersion objective (Fluor APO 60X/1.00 W, Nikon). Recordings from individual GPe neurons were performed with patch electrodes (impedance, 3–8 MΩ) fabricated from borosilicate glass capillaries (GC150F10; Warner Instruments, Hamden, CT, USA) pulled with a horizontal puller (P-97; Sutter Instruments, Novato, CA, USA). For whole-cell voltage-clamp recordings, pipettes were filled with K-Gluconate-based internal solution containing (in mM): 135 K-gluconate, 3.8 NaCl, 1 $MgCl_2.6H_2O$, 10 HEPES, 0.1 EGTA, 0.4 Na_2GTP, 2 $Mg_{1.5}ATP$, 5 QX-314 and 5.4 biocytin (pH = 7.2, ∼292 mOsm). In some recordings performed on D2-cre mice a cesium-based solution was used containing (in mM): 135 CsCl, 3.6 NaCl, 1 $MgCl_2.6H_2O$, 10 HEPES, 0.1 Na_4EGTA, 0.4 Na_3GTP, 2 $Mg_{1.5}ATP$, 5 QX-314 and 5.4 biocytin (pH = 7.2, ∼292 mOsm). Recordings were obtained using a Multiclamp 700B amplifier and Digidata 1440A digitizer controlled by Clampex 10.3/10.6 (Molecular Devices LLC). Signals were sampled at 20 kHz and low-pass filtered at 4 kHz. Whole-cell voltage clamp recordings with CsCl and K-gluconate filled electrodes were corrected for a junction potential of −4 mV and −13 mV respectively. Series resistance was monitored throughout the experiment by voltage steps of −5 mV. Data were discarded when the series resistance changed by > 20%. After electrophysiological recordings, slices were fixed overnight in a solution of paraformaldehyde at 4% and maintained in PBS-azide at 0.2% at 4°C until immunohistochemical processing.

Please cite this article in press as: Aristieta et al., A Disynaptic Circuit in the Globus Pallidus Controls Locomotion Inhibition, Current Biology (2020), https://doi.org/10.1016/j.cub.2020.11.019

Drugs

Unless otherwise stated, all drugs were purchased from BioTechne and prepared in distilled water as concentrated stock solutions and stored at −20°C. On the day of the experiment, drugs were diluted and applied through the bath perfusion system. When necessary, GABAergic and glutamatergic antagonists were used to block the synaptic transmission (data not shown). $GABA_A$ receptors were blocked with 20 μM 4-[6-imino-3-(4-methoxyphenyl) pyridazin-1-yl] butanoic acid hydrobromide (SR95531/GABAzine). NMDA receptors were blocked with 50 μM D-(–)-2-amino-5-phosphonopentanoic acid (D-APV). AMPA/kainate receptors with 20 μM 6,7-dinitroquinoxaline-2,3-dione (DNQX disodium salt).

Optogenetic stimulation

For *in vivo* experiments, optogenetic stimulations were performed through optical fibers (multimode Fiber, 0.22NA, core diameter: 105μm, Thorlabs) implanted into the right striatum and/or STN (coordinates as above). The power at the tip of the optics fibers was always measured with a power meter (PM100D, Thorlabs) right before insertion in brain tissue. Two optogenetic stimulation protocols were used during the electrophysiological recordings in this study. The first one consisted of a 2 s long continuous blue light stimulation (0.5 mW measured at the tip of optic fiber) applied every 10sec. The 2 s preceding the light pulse was used as the baseline (i.e., OFF epoch) and was compared to the effect of the 2 s long optogenetic stimulation (i.e., ON epoch). Only neurons recorded for at least 20 laser stimulations were kept for further analyzed. The second protocol consisted of a short 10 ms blue light stimulation (0.5 mW) applied every second. For behavioral experiments, optogenetic stimulation consisted of 500 ms blue light stimulation (1 mW) applied randomly with an inter-laser interval of at least 3 s. The laser bench (Errol laser) was controlled by analog signals sent by a Power1401-3 (Cambridge Electronic Design) connected to a computer equipped with Spike2 software. For *ex vivo* optogenetic stimulation, we used a LED laser source (Prizmatix, Israel) connected to an optic fiber (core diameter: 500 μm) placed directly above the brain slice. For cell body stimulation, we used continuous 1 s long light stimulation at low intensity (4 mW). To evoke reliable synaptic transmission, single pulses or train of stimulation (20 pulses at 20Hz) of 1ms duration at full power (90 mW) were used in order to maximize axon terminal depolarization and efficient release of neurotransmitter[62].

Juxtacellular labeling

In this study, we performed juxtacellular labeling to identify the location of the recorded unit as previously described[23,63]. Briefly, the recorded unit was stimulated by a current pulse of 250ms long (50% duty cycle, 1-10 nA) sent through the recording electrode by axoClamp 2B (in bridge mode; Molecular Devices). Then, the location and the molecular profile of the labeled neurons were determined by histological verification.

Histology

At this end of recording day, the mice were sacrificed with an overdose of pentobarbital sodium (150 mg/Kg, i.p.; Axience). An intracardiac perfusion (PBS 0.01mM following by formaldehyde 4%) was then performed for further histological validations. The brain was kept overnight in a solution of PBS 0.01 mM/formaldehyde 4% (v/v; CAT#20909.330, VWR) and then cut in 50 μm slices with a vibratome (VT1000, Leica Microsystemes). To reveal the juxtacellularly labeled neurons, the slices were incubated overnight in a solution of PBS 0.01 mM/Triton X-100 0.3% (v/v; CAT#T9284, Sigma-Aldrich) containing streptavidine-CY3 Zymax (1/1000, v/v; CAT#438315, Life Technologies). The slices were then washed in PBS 0.01 mM before mounting onto slides in Fluoromount medium (Cliniscience). Additional staining was performed through indirect immunofluorescence staining using primary and fluorescent secondary antibodies. For all immunostainings, the slices were incubated overnight in a solution of PBS 0.01mM / Triton X-100 0.3% (v/v) containing the primary antibody. The slices were then washed 3 times in PBS 0.01 mM, incubated 4h in a solution of PBS 0.01 mM / Triton X-100 0.3% (v/v) containing the secondary antibody, washed again in PBS 0.01 mM and mounted onto slides in Fluoromount medium. The primary antibodies used in this study were: the rabbit anti-Nkx2.1 (or anti-TTF-1, 1/500, v/v; CAT#H-190, Santa Cruz), the rabbit anti-preproenkephalin (1:5000, LifeSpan Biosciences, LS-C23084), and goat anti-FoxP2 (1/500, v/v; CAT#N-16, Santa Cruz). The immunolabelling for the preproenkephalin was optimized using the heat-treatment antigen retrieval method as described previously[23]. The secondary antibodies used were: Alexa Fluor® 488 donkey anti-chicken (1/500, v/v; CAT#703-545-155, Jackson ImmunoResearch), CY5-conjugated donkey anti-rabbit (1/500, v/v; CAT#711-175-152, Jackson ImmunoResearch), and Brilliant Violet421-conjugated donkey anti-goat (1/500, v/v; CAT#705-675-147, Jackson ImmunoResearch).

To reveal biocytin-filled neurons after *ex vivo* recordings, brain slices were incubated overnight in a solution of PBS 0.01 mM/Triton X-100 0.3% (v/v; CAT#T9284, Sigma-Aldrich) containing streptavidine-488, (1/500; Cat#S11223; Life technologies), or streptavidine-557 (1/1000; Cat# NL999, R&D system). Additional staining was performed as for the *in vivo* histology (see above), but with only 2 hours of incubation with the secondary antibody. The primary antibodies used in this study were: the rabbit anti-Nkx2.1 (same ref as above), goat anti-FoxP2 (same ref as above), Rabbit anti-RFP (1/1000; Cat# R10367, Life technologies), Rat anti-RFP (1/500, v/v; Cat#5f8, Chromotek), Mouse anti-GFP (1/600; Cat#11814460001, Roche). The secondary antibodies used were: Alexa Fluor Donkey anti-Rabbit 488 (1/500, v/v; Cat#A21206, Life technologies), Alexa Fluor Donkey anti-Mouse 488 (1/500, v/v; Cat#A 21202, Life technologies), Alexa Fluor Donkey anti-Rabbit 568 (1/500 v/v; Cat#A11075, Life technologies), Alexa Fluor Donkey anti-Rat 568 (1/500 v/v; Cat#A11077, Invitrogen), Alexa Fluor Donkey anti-Rat 594 (1/500 v/v; Cat# A21209, Life technologies), Alexa Fluor Donkey anti-Goat 647 (1/500; Cat#A21447, Life technologies). The slices were then washed in PBS 0.01 mM before mounting

Please cite this article in press as: Aristieta et al., A Disynaptic Circuit in the Globus Pallidus Controls Locomotion Inhibition, Current Biology (2020), https://doi.org/10.1016/j.cub.2020.11.019

onto slides in vectashield medium (CAT#H-1000, Vector laboratories). The low magnification images were acquired with an epifluorescence microscope (Axio Imager 2, Zeiss). The high magnification images were acquired with a confocal microscope (Leica TCS SP8) head mounted on an upright stand DM6 FS (Leica Microsystems, Mannheim, Germany) with a HC Plan Apo CS2 63X oil NA 1.40 objective and equipped with a motorized XY stage, and a galvanometric stage for fast Z acquisition. The confocal is equipped with four laser lines (405 nm, 488 nm, 552 nm and 638 nm), a conventional scanner (10-1800 Hz), and detectors (two internal PMT and two internal hybrid detectors). The images were further extracted using Fidji[64].

Behavioral locomotion experiments

Mice were daily trained to walk continuously for 5 minutes on a motorized treadmill belt (BiosebLab) running at 15cm/s for at least one week before the beginning of optogenetic experiments. During the experiments, the locomotor sequences were video capture (250 frames/s) bilaterally using a pair of high speed cameras (Basler ac 1920-150uc, Basler AG) mounted with Fujinon lenses (model HF16XA-5M) and synchronized using a trigger cable with the software Streampix (Norpix, Inc). Video recordings were stored on a computer and analyzed offline.

QUANTIFICATION AND STATISTICAL ANALYSIS

Data analysis of electrophysiological recordings

In vivo recordings

All data processing (spike sorting and ECoG filtering) were realized offline with Spike2 software (Cambridge Electronic Design). Peristimulus time histograms (PSTH) of each spike trains were generated using spike2 and a custom MATLAB® script for the 2 s long (width: 6 s, offset: 2 s, bin size: 50 ms) and the 10 ms light stimulation protocol (width: 0.180 s, offset: 0.03 s, bin size: 2.5 ms). A response was classified as statistically significant if the spike count values of 3 consecutive bins of light pulse delivery were < -2 standard deviation (SD) for inhibitory responses, or > 2 SD for excitatory responses. SD was measured during the baseline OFF epoch. We also analyzed in spike2 the frequency and the coefficient of variation (CV) of each spike train during OFF and ON epoch.

Ex vivo recordings

Ex vivo electrophysiological data were analyzed using ClampFit 10.3/10.6 (Molecular Devices LLC) and OriginPro (version 7 and 9; OriginLab Corporation). Spontaneous firing rate and standard deviation of interval interspike (SDisi) of GPe neurons were calculated by detection of action potentials over a period of 100-150 s[65] in ClampFit 10.3/10.6. PSTH of each spike trains for continuous 1 s or pulse train (20 pulses, 20Hz) optogenetic stimulations were generated using OriginPro with a bin size of 50 ms. Both frequency and count PSTH were generated for each spike train to evaluate the effect of the optogenetic manipulations. The magnitude of light-evoked inhibitory post-synaptic currents (IPSC) or excitatory post-synaptic currents (EPSC) were obtained by averaging 6-10 trials. Currents were then converted into conductance according to the formula ($g = i/(V_{rec}\text{-}E_{NT})$ were V_{rec} corresponds to the membrane potential of the recording and E_{NT} the reversal potential for GABA or Glutamate.

Data analysis of locomotion

The video frames corresponding to period of laser stimulation were extracted using home-made routines based on the OpenCV-python library. The locomotor activity of the animal measured on the treadmill was obtained from a frame by frame analysis of body landmarks position (base of the tail, fore- and hindlimb toes, and nose extremity). The X-Y coordinates of the landmarks were extracted using Deep Lab Cut[66] on a linux workstation equipped with a NVIDIA GeForce RTX 2080TI graphic card. Before any further data processing, the Deep Lab Cut labeling output was then checked for errors of detections and corrected by first comparing the detections from the left and right camera frames. In addition, a second step of correction included the replacement of labeling that yielded to an instantaneous velocity above 28 cm/s (measured as being the maximal velocity reachable by the mouse in our conditions) by the averaged value measured in the time window covering 120 ms before and after the misdetection. Two of the foretold body landmarks (Nose extremity and Tail base) were chosen for quantification purposes. The velocity corresponding to each frame (accounting for 4 ms of the movement) was calculated using the displacement along the treadmill axis (averaged over the right and left labels and body landmarks) starting 60 ms before and finishing 60 ms after. This particular 120 ms window size in addition to a moving average of window size 20 ms that was performed after the velocity calculation assured minimizing the small velocity fluctuations captured in the measurements. The mean velocity was calculated for all the frames in a 500 ms time window preceding and following the laser onset. The average velocity averaged over the laser-OFF and laser-ON period has been reported as representations of the velocity in these periods.

Statistics

Experimental data were analyzed using the computer program GraphPad Prism (v8.4.3, GraphPad Software, Inc). Data in the figures are presented as the median and interquartile range unless otherwise stated. Boxplots (central line: median; box: 25%–75%; whiskers: min-max) were used to illustrate sample distributions with individual values represented by circles or individual lines. Group data in the text and the Tables S1 and S2 are presented as mean ± standard error of the mean (SEM). For dependent sample, the paired t test was used excepts if the normality distribution test failed (Shapiro-Wilk test, $p < 0.05$). In the latter case, the Wilcoxon Signed Rank

Please cite this article in press as: Aristieta et al., A Disynaptic Circuit in the Globus Pallidus Controls Locomotion Inhibition, Current Biology (2020), https://doi.org/10.1016/j.cub.2020.11.019

(WSR) test was used. For independent samples, we applied the normality (Shapiro-Wilk test) and equal variance tests. A Mann-Whitney U (MWU) test was used when the distributions were normal and the group variances were equal. Contingency was assessed using Fisher's exact test. For multiple repeated-measured group comparisons, the Friedman test was used, followed by Dunn's post hoc test. For behavioral analysis, two-tailed, non-parametric statistical comparisons were made using Wilcoxon Signed Rank test (WSR) with Bonferroni correction to compare the OFF versus ON average velocities measured within each animal group. Furthermore, the non-parametric Mann–Whitney U (MWU) test for unpaired data was used to compare the average laser-ON velocities between the ChR2 and the eYFP control groups. The level of statistical significance was set at $p < 0.05$.

Current Biology, Volume *31*

Supplemental Information

A Disynaptic Circuit in the Globus Pallidus Controls Locomotion Inhibition

Asier Aristieta, Massimo Barresi, Shiva Azizpour Lindi, Grégory Barrière, Gilles Courtand, Brice de la Crompe, Lise Guilhemsang, Sophie Gauthier, Stéphanie Fioramonti, Jérôme Baufreton, and Nicolas P. Mallet

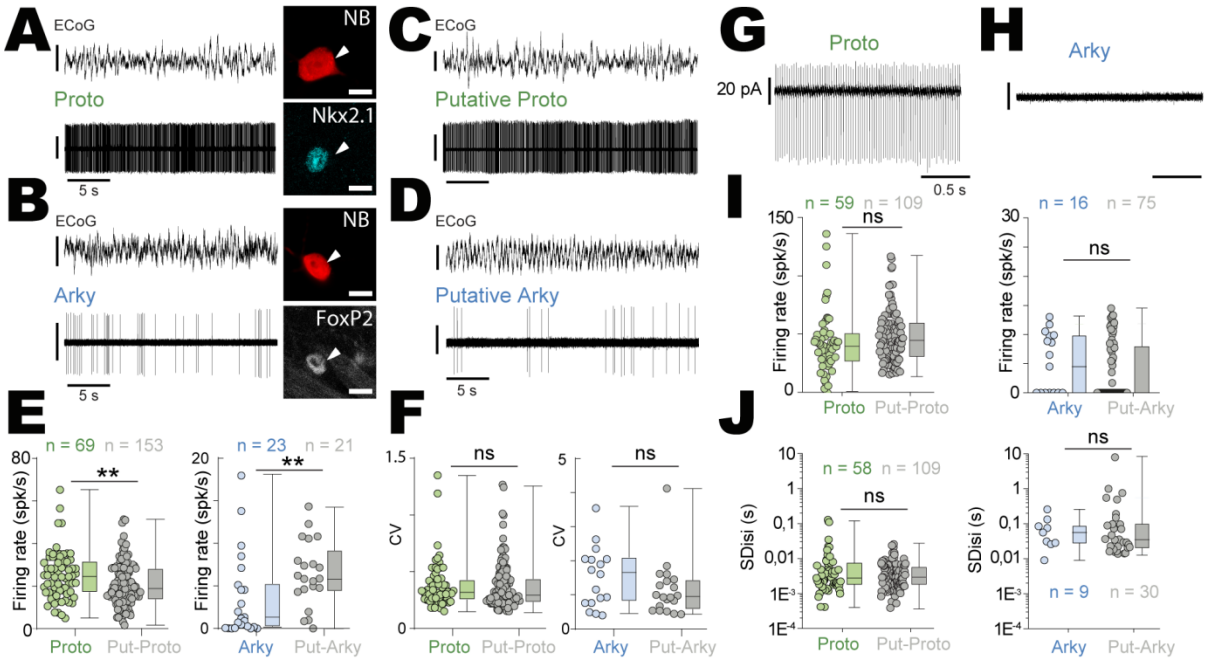

Figure S1. ***In vivo*** **and** ***ex vivo*** **electrophysiological properties of labelled** ***vs.*** **putative prototypic and arkypallidal neurons. Related to Figure 1.** ***(A, B)*** Raw *in vivo* electrophysiological traces of identified prototypic ***(A)*** and arkypallidal ***(B)*** GPe neurons recorded simultaneously with the ECoG activity. Neuronal identity was confirmed with juxtacellular neurobiotin labelling and immunodetection for the expression of Nkx2.1 for prototypic (top) or FoxP2 for arkypallidal neurons (bottom), scale bars: 10μm. ***(C, D)*** Raw *in vivo* electrophysiological recordings of putative prototypic ***(C)*** and arkypallidal GPe ***(D)*** neurons with the corresponding ECoG activity. ***(E, F)*** Comparison of the *in vivo* firing rate ***(E)*** and coefficient of variation (CV, ***F)*** for juxtacellularly labelled vs. unidentified prototypic (left) and arkypallidal (right) GPe neurons recorded *in vivo*. ***(G, H)*** Raw *ex vivo* spontaneous activity of identified prototypic ***(G)*** and arkypallidal ***(H)*** GPe neurons. ***(I, J)*** Comparison of the *ex vivo* firing rate ***(I)*** and interspike interval standard deviation (SD_{ISI}, ***J***) for identified vs. putative prototypic (left) and arkypallidal (right) neurons. ** p<0.01, ns: not significant. See Table S2 for more details and statistical information.

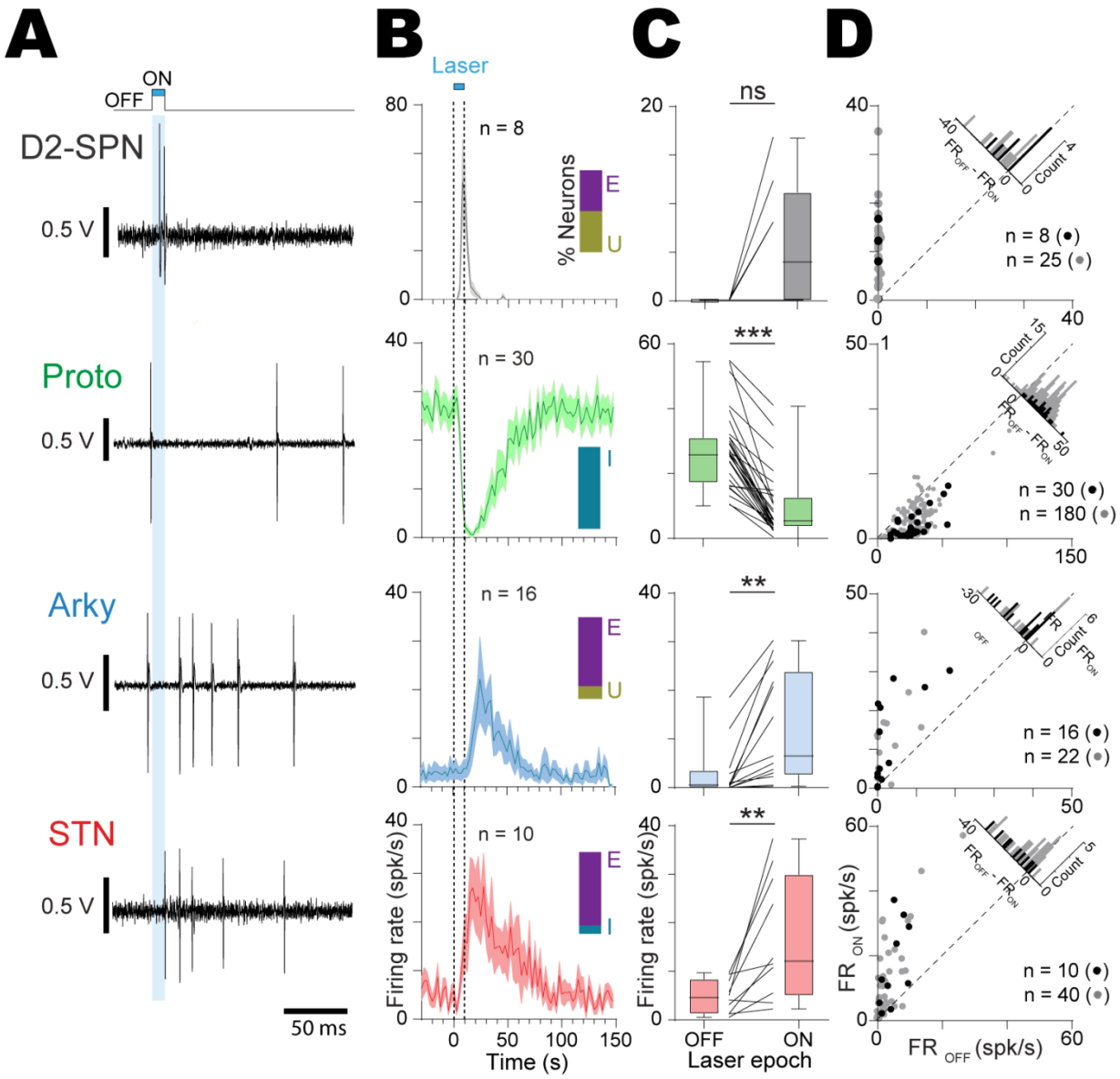

Figure S2. Short-duration opto-activation of D2-SPNs induced opposing effects on prototypic and arkypallidal neurons. Related to Figure 1. ***(A)*** Typical examples of *in vivo* single-unit activity for one juxtacellularly labelled D2-SPN, prototypic, arkypallidal, and STN neurons during D2-SPN opto-activation (10 ms blue light pulses). ***(B)*** Population PSTH (bin size: 2.5 ms) of all the juxtacellularly labelled D2-SPN (n= 8, grey), prototypic (n= 30, green), arkypallidal (n= 16, blue), and STN neurons (n= 10, red) during opto-activation of D2-SPN. ***(C)*** Box-and-whisker plots representing the average firing rate of all the labelled D2-SPNs (grey), prototypic (green), arkypallidal (blue), and STN neurons (red) during OFF *vs.* ON laser stimulation of D2-SPNs. ***(D)*** Scatter plots representation of juxtacellularly labelled (black dots) and putative (grey dots) D2-SPN, prototypic, arkypallidal, and STN neurons during D2-SPN ON/OFF opto-stimulation. Group data represents mean ± SEM, box-and-whisker plots indicate median, first and third quartile, min and max values. ** p<0.01, *** p<0.001, ns: not significant. See Table S2 for more details and statistical information.

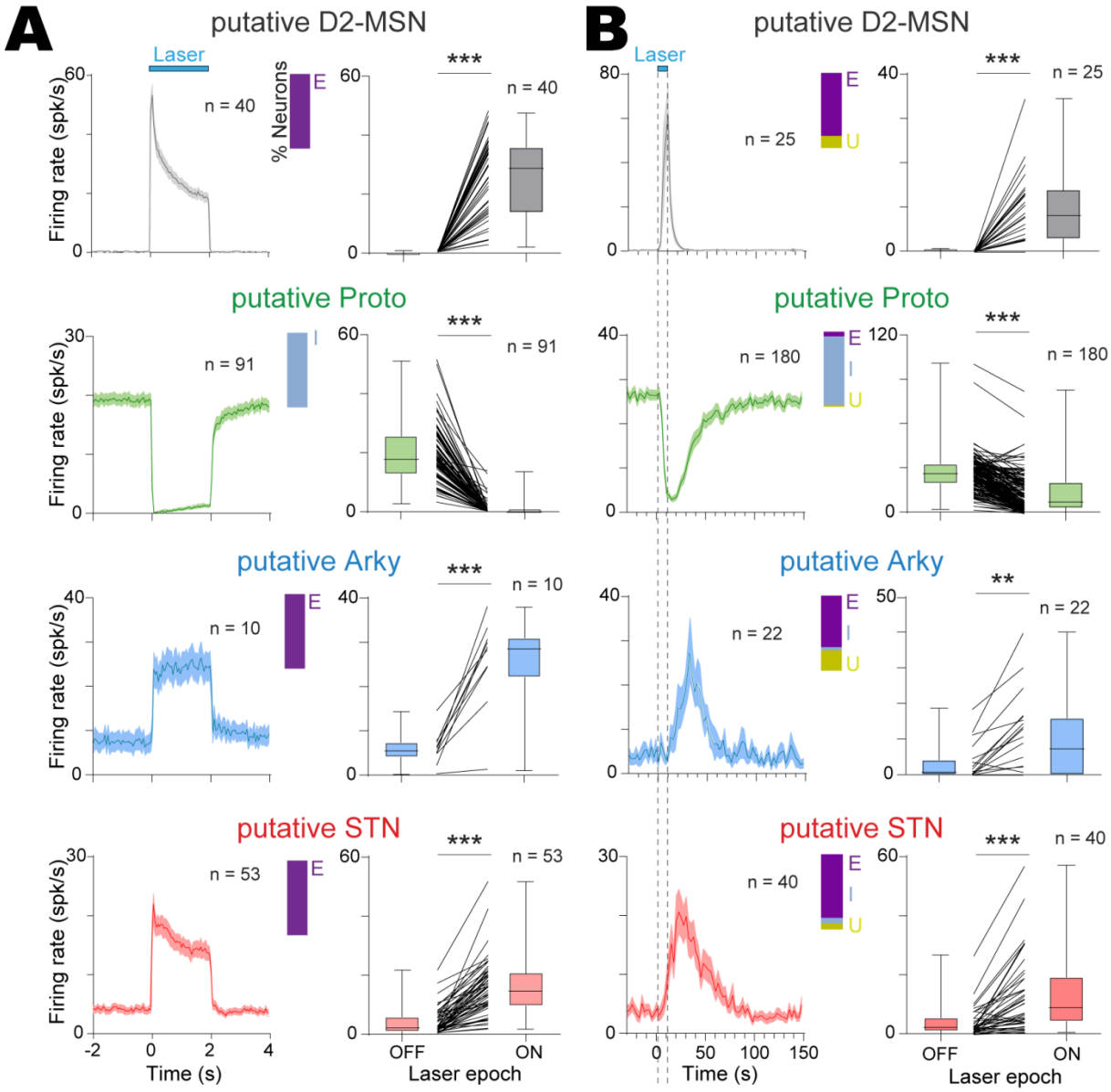

Figure S3. Opto-activation of D2-SPNs induced opposite effects in putative prototypic and putative arkypallidal neurons. Related to Figure 1. ***(A, B)*** Population PSTH (left) and average firing rate responses (right) calculated during a 2s long (***A***, bin size: 50 ms) or a 10 ms short (***B***, bin size: 2.5 ms) opto-excitation of D2-SPNs for putative D2-SPN (grey), prototypic (green), arkypallidal (blue), and STN neurons (red). Group data represents mean ± SEM, box-and-whisker plots indicate median, first and third quartile, min and max values. ** p<0.01, *** p<0.001. See Table S2 for more details and statistical information.

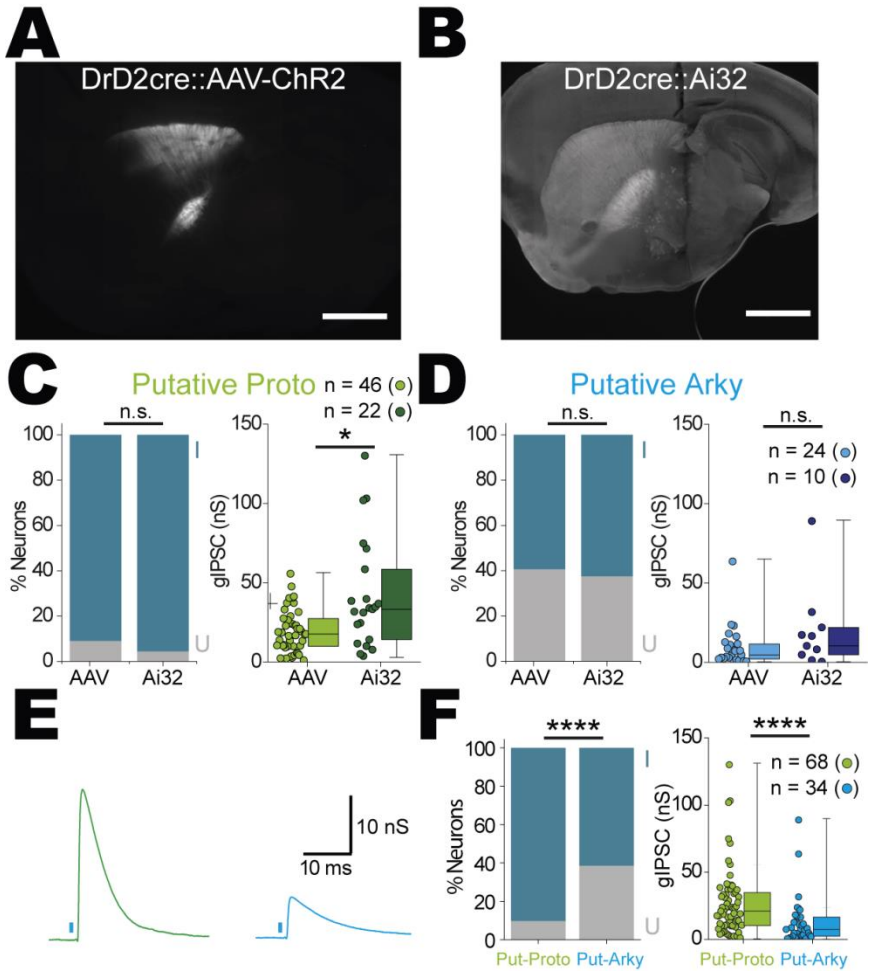

Figure S4. ***Ex vivo*** **characterization of D2-SPN inputs onto putative GPe neurons. Related to Figure 1.** ***(A, B)*** Epifluorescent images illustrating the virus-induced ChR2-eYFP expression in sub-population of D2-SPNs (***A***) or the constitutive expression of ChR2-eYFP using D2-Cre::Ai32 mice that labelled all D2-SPNs (***B***) in the striatum and their respective projections to the GPe (scale: 0.5 mm). ***(C)*** Bar graph representing the percentage of IPSC-recipient (right) and the averaged IPSC conductance (left) for all the putative prototypic neurons recorded in D2-Cre::AAV-ChR2-eYFP mice (AAV and light green) or in D2-Cre::Ai32 mice (Ai32 and dark green). ***(D)*** Bar graph representing the percentage of IPSC-recipient (right) and the averaged IPSC conductance (left) for all the putative arkypallidal neurons recorded in D2-Cre::AAV-ChR2-eYFP mice (AAV and light blue) or in D2-Cre::Ai32 mice (Ai32 and dark blue). ***(E)*** Typical inhibitory post-synaptic currents (IPSCs) recorded in putative prototypic (green) or arkypallidal (blue) neurons during the laser-stimulation (1ms pulse) of D2-SPN axon terminals in D2-Cre mice injected with an AAV-ChR2 in the striatum. ***(F)*** Bar graph representing the percentage of IPSC-recipient (left) and the averaged magnitude of IPSC conductance (right) measured in putative prototypic and arkypallidal neurons. * $p<0.05$, **** $p<0.0001$, ns: not significant. See Table S2 for more details and statistical information.

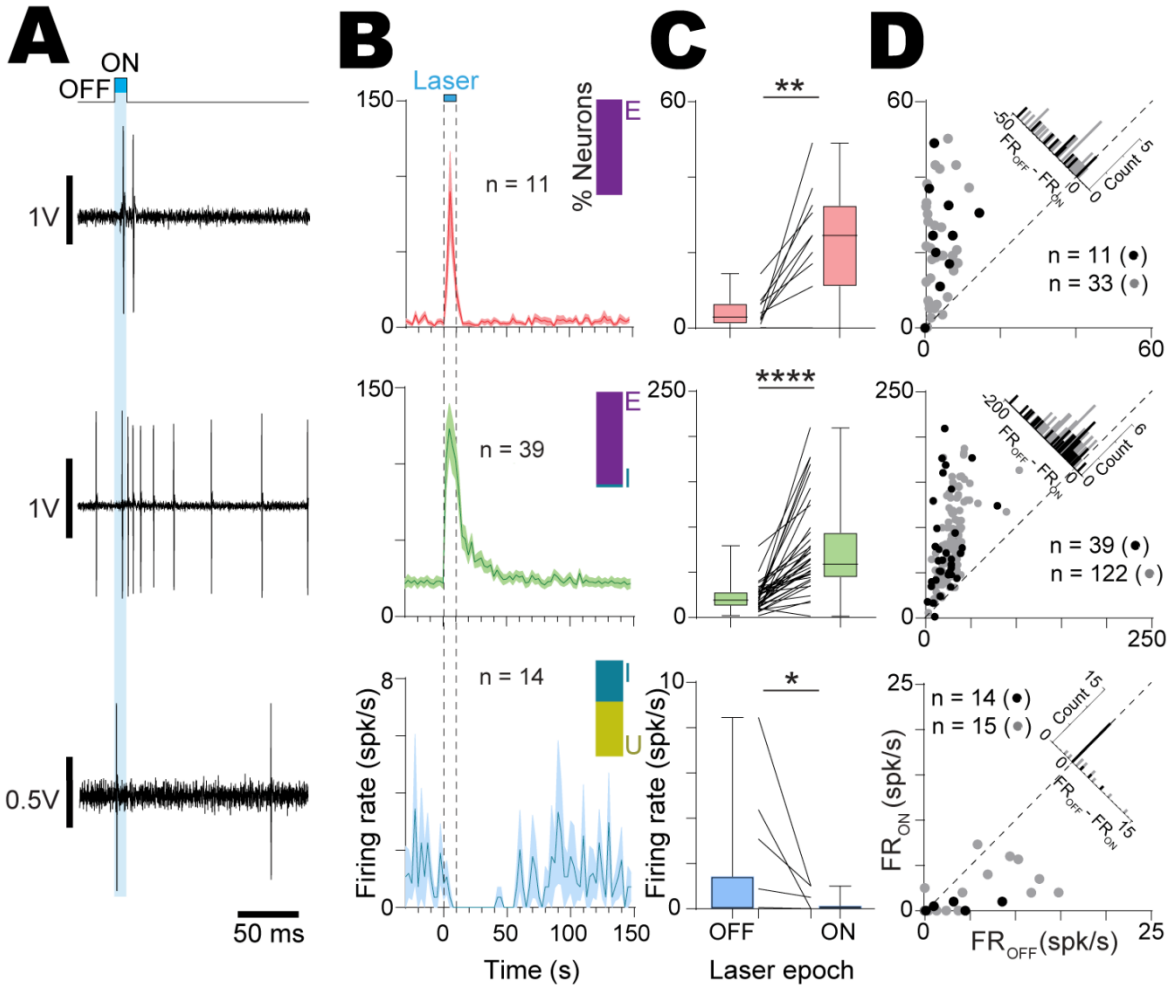

Figure S5. Short-duration opto-activation of STN neurons induced opposite effects on prototypic and arkypallidal neurons *in vivo*. Related to Figure 3. ***(A)*** Representative examples of *in vivo* single-unit activity for one juxtacellularly labelled STN, prototypic, and arkypallidal neurons during STN opto-activation (10 ms blue light pulses). ***(B)*** Population PSTH (bin size: 2.5 ms) of all juxtacellularly labelled STN (n= 11), prototypic (n= 39) and arkypallidal neurons (n= 14) during opto-activation of STN neurons. The inset bar plot represents the percentage of neurons excited (E), inhibited (I) and unaffected (U) by the light stimulation. ***(C)*** Box-and-whisker plots representing the average firing rate of all the labelled STN (red), prototypic (green) and arkypallidal (blue) neurons during OFF *vs.* ON laser stimulation of STN neurons. ***(D)*** Scatter plots representation of juxtacellularly labelled (black dots) and putative (grey dots) STN, prototypic and arkypallidal neurons during STN neurons ON/OFF opto-stimulation. Group data represents mean ± SEM, box-and-whisker plots indicate median, first and third quartile, min and max values.* $p<0.05$, ** $p<0.01$, **** $p<0.0001$. See Table S2 for more details and statistical information.

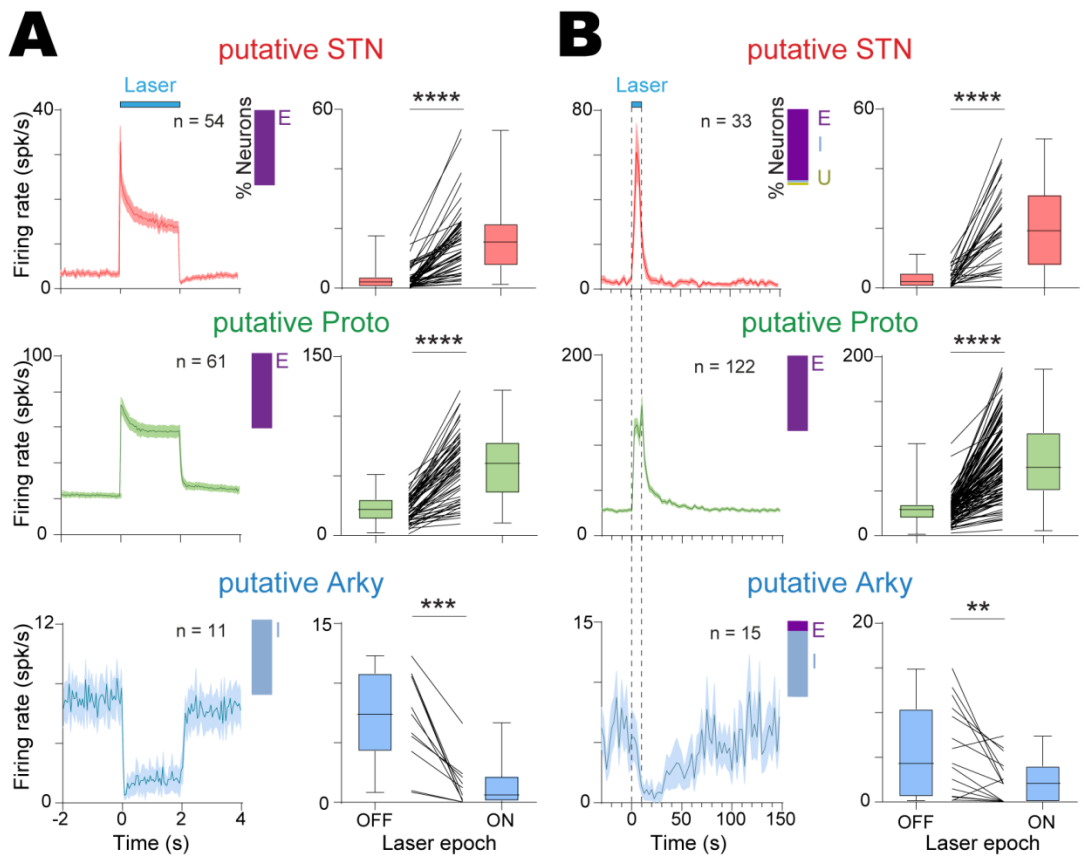

Figure S6. Opto-activation of STN neurons induced opposite effects on putative prototypic and putative arkypallidal neurons *in vivo*. Related to Figure 3. ***(A, B)*** Population PSTH (left) and averaged firing rate responses (right) calculated during a 2s long (***A***, bin size: 50 ms) or a 10 ms short (***B***, bin size: 2.5 ms) opto-excitation of STN neurons for putative STN (red), prototypic (green), arkypallidal (blue) neurons. The inset bar plots represent the percentage of neurons excited (E), inhibited (I) an unaffected (U) by the light stimulation. Group data represents mean ± SEM, box-and-whisker plots indicate median, first and third quartile, min and max values. ** p<0.01, *** p<0.001, **** p<0.001. See Table S2 for more details and statistical information.

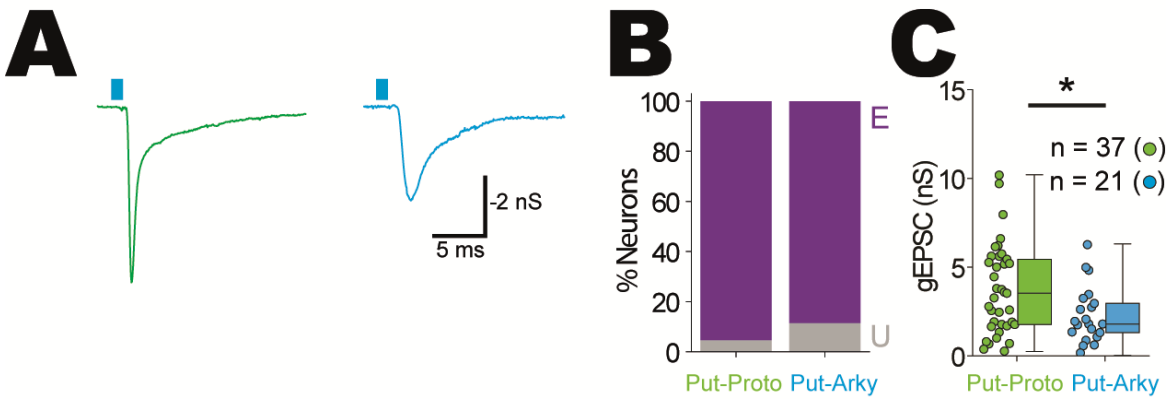

Figure S7. Opto-activation of STN inputs induced excitatory post-synaptic currents in putative GPe neurons *ex vivo*. Related to Figure 3. ***(A)*** Representative excitatory post-synaptic currents (EPSCs) evoked by light-activation (1ms) of STN axon terminals of Vglut2-Cre mice injected in the STN with an AAV-DIO-ChR2. ***(B)*** Bar graph representing the percentage of EPSC-recipient (purple) putative prototypic and arkypallidal neurons. E: excited; U: unchanged. ***(C)*** Population data depicting the greater magnitude of EPSC conductance in putative prototypic compared to arkypallidal neurons. * $p<0.05$. See Table S2 for more details and statistical information.

Figure	Parameter	n (mice/neurons)	Data Type	Data Value (mean ± SEM)	Statistical test	significance level
1D	D2-SPNs Firing rate	(4/8)	OFF	0.081 ± 0.058	Wilcoxon signed rank test	*p*=0.0078
			ON	31.88 ± 3.11		
1E	Proto Firing rate	(24/36)	OFF	26.12 ± 1.70	Paired t test	t=13.79, *p*<0.0001
			ON	1.02 ± 0.34		
1F	Arky Firing rate	(13/14)	OFF	4.41 ± 1.51	Wilcoxon signed rank test	*p*=0.0002
			ON	20.83 ± 3.28		
1G	STN Firing rate	(5/10)	OFF	4.92 ± 0.98	Paired t test	t=7.036, *p*<0.0001
			ON	19.21 ± 2.39		
1J	Firing rate	(30/59)	Proto	42.51 ± 3.48	Mann-Whitney U test	*U=44.5*, *p*<0.0001
		(14/16)	Arky	5.2 ± 1.27		
	SDisi	(29/58)	Proto	0.0109 ± 0.0034	Mann-Whitney U test	*U=32*, *p*<0.0001
		(9/9)	Arky	0.0775 ± 0.0256		
1L	Input-recipient D2-SPN	(22/57)	% of Proto	94.74 %	*Fischer exact test*	*p*=0.0146
		(12/12)	% of Arky	66.67 %		
1L	Conductance	(28/54)	Proto	24.28 ± 2.49	Mann-Whitney U test	*U=18*, *p*<0.0001
		(8/8)	Arky	3.487 ± 1.08		
2D	STN Firing rate	(8/74)	OFF	6.12 ± 0.55	Wilcoxon signed rank test	*p*<0.0001
			ON	1.11 ± 0.23		
2I	Proto Firing rate	(10/25)	OFF	28.18 ± 1.79	Friedman test with Dunn's multiple comparisons	Off *vs.* D2: Z=6.408, *p*<0.0001 Off *vs.* STN: Z=3.232, *p*=0.0074 Off *vs.* D2+STN: Z=6.792, *p*<0.0001 D2 *vs.* STN: Z=3.177, *p*=0.0089 D2 *vs.* D2+STN: Z=0.3834, *p*>0.9999 STN *vs.* D2+STN: Z=3.560, *p*=0.0022
			D2	0.57 ± 0.26		
			STN	10.29 ± 1.52		
			D2 + STN	0.44 ± 0.21		
2J	Arky Firing rate	(7/9)	OFF	3.31 ± 1.62	Friedman test with Dunn's multiple comparisons	Off *vs.* D2: Z=3.651, *p*=0.0016 Off *vs.* STN: Z=1.643, *p*=0.6021 Off *vs.* D2+STN: Z=3.834, *p*=0.0008 D2 *vs.* STN: Z=2.008, *p*=0.2677
			D2	24.50 ± 4.51		

			STN	9.29 ± 2.26		D2 *vs.* D2+STN: Z=0.1826, *p*>0.9999 STN *vs.* D2+STN: Z=2.191, *p*=0.1708
			D2 + STN	20.95 ± 2.60		
3E	STN Firing rate	(5/11)	OFF	3.63 ± 1.26	Wilcoxon signed rank test	*p*=0.001
			ON	16.12 ± 2.44		
	Proto Firing rate	(21/32)	OFF	23.68 ± 2.23	Wilcoxon signed rank test	*p*<0.0001
			ON	75.56 ± 6.98		
	Arky Firing rate	(9/9)	OFF	2.16 ± 1.07	Wilcoxon signed rank test	*p*=0.0078
			ON	0.16 ± 0.15		
3J	Input-recipient STN	(4/16)	% of Proto-GPe	100%	Fischer exact test	*p*=1
		(7/9)	% of Arky-GPe	100%		
3J	Conductance	(4/16)	Proto-GPe	5.429 ± 0.81	Mann-Whitney U test	*U=11*, *p*=0.0002
		(7/9)	Arky-GPe	1.423 ± 0.45		
4F	Arky Firing rate	(7/9)	OFF	3.95 ± 1.39	Friedman test with Dunn's multiple comparisons	Off *vs.* D2: Z=2.008, *p*=0.2677 Off *vs.* STN: Z=1.461, *p*=0.8648 Off *vs.* D2+STN: Z=2.008, *p*=0.2677 D2 *vs.* STN: Z=3.469, *p*=0.0031 D2 *vs.* D2+STN: Z=0.000, *p*>0.9999 STN *vs.* D2+STN: Z=3.469, *p*=0.0031
			D2	23.56 ± 4.79		
			STN	2.73 ± 2.73		
			D2 + STN	37.94 ± 14.11		
4G	Arky Firing rate	(12/13)	OFF	1.57 ± 0.94	Friedman test with Dunn's multiple comparisons	Off *vs.* D2: Z=2.431, *p*=0.0904 Off *vs.* STN: Z=1.139, *p*>0.9999 Off *vs.* D2+STN: Z=1.747, *p*=0.4838 D2 *vs.* STN: Z=3.570, *p*=0.0021 D2 *vs.* D2+STN: Z=0.6836, *p*>0.9999 STN *vs.* D2+STN: Z=2.886, *p*=0.0234
			D2	8.85 ± 2.38		
			STN	2.23 ± 2.23		
			D2 + STN	14.56 ± 2.23		
5E	Proto Firing rate	(5/12)	OFF	17.81 ± 5.61	Wilcoxson Signed Rank	*p*=0.0005
			ON	97.14 ± 17.10		
5F	Arky Firing rate	(5/8)	OFF	10.28 ± 1.46	Wilcoxson Signed Rank	*p*=0.0078
			ON	3.34 ± 0.97		

5G	Conductance	(4/9)	Proto-GPe	6.17 ± 1.5	Mann-Whitney U test	p=0.2775
		(4/10)	Arky-GPe	4.38 ± 1.07		
6E	Arky Firing rate	(6/10)	OFF	11.86 ± 4.15	Wilcoxson Signed Rank	p=0.0002
			ON	82.71 ± 14.93		
6F	Proto Firing rate	(7/25)	OFF	40.18 ± 4.41	Wilcoxson Signed Rank	p=0.523
			ON	41.14 ± 4.38		
6I	Proto Firing rate	(3/61)	OFF	28.256 ± 1.290	Paired *t* test	t=0.1571, p=0.8757
			ON	28.049 ± 1.981		
Figure	**Parameter**	**n (mice/laser stim)**	**Data Type**	**Data Value**	**Statistical test**	**significance level**
7I	**Average velocity**	D2-Cre :: AAV-ChR2 (7/748)	OFF	0.684±0.273	Wilcoxon signed-rank test	ON-ChR2 vs. OFF-ChR2: $Z=47397$, $p=10^{-56}$
			ON	-6.218±0.305		
		D2-Cre :: AAV-eYFP (2/227)	OFF	1.259±0.556	Mann-Whitney U test	ON-ChR2 vs. ON-Control: $U=49134$, $p=10^{-22}$
			ON	0.189±0.520		
		Vglut2-Cre :: AAV-ChR2 (7/778)	OFF	0.142±0.245	Wilcoxon signed-rank test	ON-ChR2 vs. OFF-ChR2: $Z=143970$, p=0.23
			ON	0.327±0.301		
		Vglut2-Cre :: AAV-eYFP (2/158)	OFF	0.850±0.530	Mann-Whitney U test	ON-ChR2 vs. ON-Control: $U=58789$, p=0.19
			ON	-0.064±0.526		
		FoxP2-Cre :: AAV-ChR2 (6/711)	OFF	0.566±0.179	Wilcoxon signed-rank test	ON-ChR2 vs. OFF-ChR2: $Z=1395$, $p=10^{-114}$
			ON	-15.535±0.139		
		FoxP2-Cre :: AAV-eYFP (2/223)	OFF	0.448±0.460	Mann-Whitney U test	ON-ChR2 vs. ON-Control: $U=4559$, $p=10^{-100}$
			ON	-0.163±0.444		

Table S1. Statistical analyses. Related to the data presented in Figure 1 to 7.

Figure	Parameter	n (mice/neurons)	Data Type	Data Value (mean ± SEM)	Statistical test	significance level
S1E	Proto Firing rate	(45/68)	labelled	24.97 ± 1.38	Mann-Whitney U test	U=3986, *p*=0.0065
		(46/152)	putative	20.59 ± 0.81		
S1E	Arky Firing rate	(22/23)	labelled	3.532 ± 1.02	Mann-Whitney U test	U=127.5, *p*=0.0066
		(19/21)	putative	6.41 ± 0.83		
S1E	Firing rate	(45/68)	Proto-GPe labelled	24.97 ± 1.38	Mann-Whitney U test	U=42, *p*<0.0001
		(22/23)	Arky-GPe labelled	3.532 ± 1.02		
S1E	Firing rate	(46/15)	Proto-GPe putative	20.59 ± 0.81	Mann-Whitney U test	U=219, *p*<0.0001
		(19/21)	Arky-GPe putative	6.41 ± 0.83		
S1F	Proto CV	(45/68)	labelled	0.371 ± 0.02	Mann-Whitney U test	U=5012, *p*=0.7217
		(46/152)	putative	0.372 ± 0.01		
S1F	Arky CV	(15/17)	labelled	1.514 ± 0.21	Mann-Whitney U test	U=126.5, *p*=0.1898
		(18/20)	putative	1.16 ± 0.18		
S1F	CV	(45/68)	Proto-GPe labelled	0.371 ± 0.02	Mann-Whitney U test	U=56.50, *p*<0.0001
		(15/17)	Arky-GPe labelled	1.514 ± 0.21		
S1F	CV	(46/152)	Proto-GPe putative	0.372 ± 0.01	Mann-Whitney U test	U=191, *p*<0.0001
		(18/20)	Arky-GPe putative	1.16 ± 0.18		
S1I	Proto Firing rate	(30/59)	labelled	42.51 ± 3.48	Mann-Whitney U test	U=2634, *p*=0.053
		(57/109)	putative	48.57 ± 2.15		
	Arky Firing rate	(14/16)	labelled	5.2 ± 1.27	Mann-Whitney U test	U=493.5, *p*=0.221
		(46/75)	putative	3.46 ± 0.54		
S1J	Proto SDisi	(29/58)	labelled	0.0109 ± 0.0034	Mann-Whitney U test	U=3080, *p*=0.786
		(57/109)	putative	0.0046 ± 0.0004		
	Arky SDisi	(9/9)	labelled	0.0775 ± 0.0256	Mann-Whitney U test	U=126, *p*=0.78
		(16/30)	putative	0.395 ± 0.262		

Figure	Parameter	n (mice/neurons)	Data Type	Data Value (mean ± SEM)	Statistical test	significance level
S2C	D2-SPNs Firing rate	(4/8)	OFF	0.018 ± 0.018	Wilcoxon signed rank test	*p*=0.1250
			ON	5.62 ± 2.33		
S2C	Proto Firing rate	(21/30)	OFF	27.14 ± 2.15	Wilcoxon signed rank test	*p*<0.0001
			ON	9.51 ± 1.79		
S2C	Arky Firing rate	(13/16)	OFF	2.54 ± 1.32	Wilcoxon signed rank test	*p*=0.0002
			ON	10.17 ± 2.84		
S2C	STN Firing rate	(5/10)	OFF	4.84 ± 1.07	Paired t test	t=3.444, *p*=0.0073
			ON	16.88 ± 4.03		
S3A	Put-D2-SPNs Firing rate	(7/40)	OFF	0.061 ± 0.025	Wilcoxon signed rank test	*p*<0.0001
			ON	25.92 ± 2.02		
S3A	Put-Proto Firing rate	(22/91)	OFF	19.39 ± 0.96	Wilcoxon signed rank test	*p*<0.0001
			ON	0.908 ± 0.263		
S3A	Put-Arky Firing rate	(9/10)	OFF	5.74 ± 1.19	Paired t test	t=6.681, *p*<0.0001
			ON	25.30 ± 3.24		
S3A	Put-STN Firing rate	(7/53)	OFF	4.07 ± 0.61	Wilcoxon signed rank test	*p*<0.0001
			ON	15.56 ± 1.31		
S3B	Put-D2-SPNs Firing rate	(7/25)	OFF	0.066 ± 0.03	Wilcoxon signed rank test	*p*<0.0001
			ON	9.34 ± 1.65		
S3B	Put-Proto Firing rate	(41/180)	OFF	26.73 ± 0.87	Wilcoxon signed rank test	*p*<0.0001
			ON	12.57 ± 0.93		
S3B	Put-Arky Firing rate	(20/22)	OFF	2.96 ± 1.08	Wilcoxon signed rank test	*p*=0.0002
			ON	9.76 ± 2.37		
S3B	Put-STN Firing rate	(7/40)	OFF	3.93 ± 0.78	Wilcoxon signed rank test	*p*<0.0001
			ON	13.14 ± 2.04		
S4C	Input recipient D2-MSN	(30/52)	% of Put-Proto/AAV	88.46 %	Fischer's exact test	*p*=0.4272
		(12/23)	% of Put-Proto/Ai32	95.65 %		
	Conductance	(25/46)	AAV	19.86 ± 1.98	Mann-Whitney U test	U=298, *p*=0.0058
		(10/22)	Ai32	41.87 ± 7.37		
S4D	Input recipient D2-MSN	(23/40)	% of Put-Arky/AAV	60%	Fischer's exact test	*p*=0.999
		(16/16)	% of Put-Arky/Ai32	62.5%		
	Conductance	(10/24)	AAV	9.9 ± 2.73	Mann-Whitney U test	U=84, *p*=0.182
		(7/10)	Ai32	20.09 ± 8.24		

Figure	Parameter	n (mice/neurons)	Data Type	Data Value (mean ± SEM)	Statistical test	significance level
S4F	Input recipient D2-MSN	(42/75)	% of Put-Proto	90.66%	Fischer's exact test	$p<0.0001$
		(39/56)	% of Put-Arky	60.71%		
	Conductance	(35/68)	Put-Proto	26.98 ± 2.98	Mann-Whitney U test	U=565, $p=0.0001$
		(17/34)	Put-Arky	12.9 ± 3.12		
S5C (Top)	STN Firing rate	(5/11)	OFF	4.29 ± 1.27	Paired t test	t=4.183, $p=0.0019$
			ON	22.36 ± 4.54		
S5C (Middle)	Proto Firing rate	(29/39)	OFF	22.39 ± 2.25	Wilcoxon signed rank test	$p<0.0001$
			ON	75.63 ± 7.97		
S5C (Bottom)	Arky Firing rate	(12/14)	OFF	1.20 ± 0.66	Wilcoxon signed rank test	$p=0.0313$
			ON	0.18 ± 0.099		
S6A (Top)	Put-STN Firing rate	(8/54)	OFF	3.31 ± 0.53	Wilcoxon signed rank test	$p<0.0001$
			ON	16.20 ± 1.52		
S6A (Middle)	Put-Proto Firing rate	(21/61)	OFF	22.05 ± 1.35	Paired t test	t=14.23, $p<0.0001$
			ON	58.51 ± 3.43		
S6A (Bottom)	Put-Arky Firing rate	(10/11)	OFF	7.02 ± 1.19	Paired t test	t=5.095, $p=0.0005$
			ON	1.36 ± 0.58		
S6B (Top)	Put-STN Firing rate	(8/33)	OFF	3.15 ± 0.53	Wilcoxon signed rank test	$p<0.0001$
			ON	20.78 ± 2.36		
S6B (Middle)	Put-Proto Firing rate	(28/122)	OFF	27.91 ± 1.19	Wilcoxon signed rank test	$p<0.0001$
			ON	82.88 ± 3.79		
S6B (Bottom)	Put-Arky Firing rate	(14/15)	OFF	5.71 ± 1.31	Paired t test	t=3.048, $p=0.0087$
			ON	2.33 ± 0.64		
S7B	Input recipient STN	(14/39)	% of Put-Proto	94.87%	*Fischer exact test*	$p=0.36$
		(11/24)	% of Put-Arky	87.5%		
S7C	Conductance	(14/37)	Proto-putative	3.74 ± 0.41	Mann-Whitney U test	U=255, $p=0.0306$
		(10/21)	Arky-putative	2.28 ± 0.34		

Table S2. Statistical analyses. Related to the data presented in Figure 1 to 7 and S1 to S7.